

RESEARCH ARTICLE OPEN ACCESS

The Upper Sedimentary Sequence of Grotta di Fumane, Northern Italy: A Micromorphological Approach to Study Imprints of Human Occupation and Paleoclimate Change

Martin Kehl^{1,2}  | Diana Marcazzan³  | Christopher E. Miller^{3,4} | Armando Falcucci⁵  | Rossella Duches⁶ | Marco Peresani^{7,8} 

¹Institute of Geography, University of Cologne, Cologne, Germany | ²Department of Geography, University of Koblenz, Koblenz, Germany | ³Institute for Archaeological Sciences and Senckenberg Centre for Human Evolution and Palaeoenvironment, University of Tübingen, Tübingen, Germany | ⁴SFF Centre for Early Sapiens Behaviour (SapienCE), University of Bergen, Bergen, Norway | ⁵Department of Geosciences, Early Prehistory and Quaternary Ecology Research Unit, Eberhard Karls University of Tübingen, Tübingen, Germany | ⁶MUSE - Museum of Sciences, Corso del Lavoro e della Scienza, Trento, Italy | ⁷Department of Humanities, Section of Prehistoric and Anthropological Sciences, University of Ferrara, Ferrara, Italy | ⁸Institute of Environmental Geology and Geoengineering, National Council of Research, Milano, Italy

Correspondence: Martin Kehl (mkehl@uni-koblenz.de) | Marco Peresani (psm@unife.it)

Received: 22 May 2023 | **Revised:** 6 February 2025 | **Accepted:** 10 February 2025

Scientific editing by Kevin Walsh.

Keywords: cave | geoarchaeology | Italian Alps | paleolithic | sedimentary process

ABSTRACT

Fumane Cave contains a sequence of natural and anthropogenic deposits documenting key transitions in the Paleolithic of Northern Italy. Open questions remain concerning the stratigraphic integrity, the formation processes, postdepositional alterations, and paleoclimatic implications of the sedimentary record. We examine these aspects through an extensive investigation based on field descriptions and micromorphological analysis of thin sections sampled during the last 25 years of excavations. Major components of the sediments are carbonate sands and limestone rubble originating from the physical breakdown of the cave roof and walls. Limited amounts of mica and quartz grains attest to weak eolian inputs. Sediments contain anthropogenic features and variable amounts of charcoal, bone, and lithic artifacts reflecting different uses of the site. Cryoturbation features observed in the field suggest an increased intensity of frost mainly after the accumulation of unit A2. This unit as well as unit A6 also show increased abundance of silt and clay cappings under the microscope, probably reflecting higher rates of snowfall and percolating meltwater during colder periods of the Last Glacial. However, limited expression of micromorphological features related to frost suggests rather modest changes in climate during the accumulation of the sequence. Overall, field descriptions and the micromorphological approach mostly corroborate the stratigraphic integrity of the sequence, underlining the high value of Fumane Cave as an archive of the late Middle to early Upper Paleolithic in Southern Europe.

1 | Introduction

The transition process from the Middle to the Upper Paleolithic (MP/UP) with the expansion of *Homo sapiens* and the demise of Neanderthals between 55,000 and 40,000 years ago (50–40 ka) has been one of the most conflicted topics in Prehistoric archaeology

in the last decades (D'Errico and Banks 2013; Greenbaum et al. 2019; Higham et al. 2014; Hublin 2015; Vaesen et al. 2021; Slimak et al. 2022; Villa and Roebroeks 2014). In this process, significant questions remain open regarding human behavior, subsistence, and above all, how cultural innovations can highlight substantial cognitive differences (Colagè and d'Errico 2020),

This is an open access article under the terms of the [Creative Commons Attribution](https://creativecommons.org/licenses/by/4.0/) License, which permits use, distribution and reproduction in any medium, provided the original work is properly cited.

© 2025 The Author(s). *Geoarchaeology* published by Wiley Periodicals LLC.

represented across the archaeological record by the appearance of the Initial Upper Paleolithic and other techno-complexes such as the Châtelperronian and the Uluzzian (Hublin 2015; Zilhão et al. 2024).

In order to further elucidate these complex issues, new data from sites with high temporal resolution and reliable sedimentary contexts are needed. Among these, the Fumane Cave (or Grotta di Fumane) is outstanding. It is a key site for the study of the Middle Paleolithic and the MP/UP transition in the Northern Mediterranean and of the origin of behavioral modernity in Europe (Peresani 2022).

The rich archaeological assemblages of the Late Mousterian and Proto-Aurignacian at Fumane are included in a finely stratified sedimentary sequence. An Uluzzian layer was discovered as well (Peresani et al. 2016), representing the northernmost occurrence of this techno-complex along with the record from Riparo Broion (Peresani et al. 2019). The stratigraphic sequence documents repeated and high-frequentation occupations of the cave, corroborated by radiocarbon dates (Peresani et al. 2008; Higham et al. 2009; Douka et al. 2014; Marín-Arroyo et al. 2023). Although the archaeological artifacts of Fumane Cave have been extensively studied, yielding important findings on human behavior (Peresani 2022 and references therein), less information has been published on its sedimentary record and microstratigraphy, which is indispensable to assess the role of natural or anthropogenic deposition processes and the stratigraphic integrity of the archaeological sequence.

Here, we attempt to decipher diachronic and spatial changes in processes of sediment accumulation and postdepositional disturbance at Fumane Cave using field evidence and a micromorphological approach. Micromorphology, or the study of intact monoliths of sediments and soils under magnification, has recently received considerable attention and is now an indispensable method for describing archaeological sediment sequences of caves, rockshelters, and open-air sites (e.g., Courty et al. 1989; Goldberg and Macphail 2006; Goldberg and Berna 2010; Nicosia and Stoops 2017). Micromorphology is used to clarify the nature of natural or anthropogenic sediment components and their spatial organization. Processes of sediment deposition and postdepositional alteration can then be deduced from structural and compositional features (e.g., Courty and Vallverdu 2001; Mallol et al. 2010; Van der Meer and Menzies 2011; Karkanis and Goldberg 2013; Stoops et al. 2018). Important aspects are the distinction between undisturbed and reworked layers (Courty 2001; Kehl et al. 2016) and the detection of trampled horizons via differential degrees of compaction or presence of crushed materials (e.g., Goldberg et al. 2009; Linstädter and Kehl 2012; Estévez et al. 2014; Alcaraz-Castaño et al. 2017). Overall, the microstratigraphic approach has become a highly valuable tool to unravel the stratigraphic sequences of Paleolithic sites (e.g., Miller et al. 2013; Karkanis et al. 2015; Mallol and Mentzer 2017).

During the last 25 years (1996–2019) of excavation of the Fumane MP-UP sedimentary sequence, a large number of structurally intact sediment samples have been collected and used for the preparation of thin sections. The first micromorphological observations on the whole Fumane sequence were presented by

Cremschi et al. (2005), who related admixtures of silt size quartz and feldspar grains in the cave deposits to eolian inputs. Silt cappings on coarse materials and platy microstructure were interpreted as effects of former frost action. In addition, the presence of illuvial clay coatings in the dolomitic sands of the lowest strata (macro-unit S) above the bedrock was noted. A. Danti (in Peresani et al. 2011) analyzed a set of thin sections prepared for Mousterian unit A6. Coarse cappings and platy or banded microstructures were identified and related to post-depositional ice-lensing. The expression of such microstructures was found to depend on the location of sampling, where samples from the interior of the cave showed more frequent frost features than those from further outside. Marcazzan et al. (2023) focused on the micromorphological properties of purported combustion features. Five different types of anthropogenic sediment features were thus identified in Fumane Cave, that is, hearths, dumping areas, occupation horizons, laminated anthropogenic features, and isolated concentrations of anthropogenic materials. Hearths and dumping areas are indicative of short events of usage, whereas formation of the three other classes is probably related to longer lasting activities on a living floor partly compacted by trampling.

A comprehensive micromorphological study of units A10 to A1 as well as D3 and D1 of the sedimentary sequence chronologically framed in the marine isotope stages 3 and 2 (MIS3–MIS2) is within the scope of this paper, in which we exclude samples from the purported combustion features studied by Marcazzan et al. (2023). Our objectives are to gain further insights into the composition and structure of the different sedimentary units and thereby on the formation processes of the MP-UP sequence at Fumane. The degree of weathering, pedogenic transformations, or postdepositional modifications are described and possible indicators of paleoenvironmental change such as eolian inputs of silt grains and frost signatures are assessed. In addition, the significance of anthropogenic versus natural accumulation processes is evaluated. Besides micromorphological data, we also provide detailed field descriptions of the sedimentary sequence, compiled over the last decades of excavation. Finally, we attempt to bring the two scales of observation together to draw conclusions on possible diachronic changes in sediment accumulation and alteration processes.

2 | Geographical Setting, Archaeological Site, and Sedimentary Sequence

Fumane Cave is located on the southern side of the Alps in the Monti Lessini region of the Venetian prealps (Figure 1) and situated on the west facing slope of the Fumane valley at an altitude of 350 m above sea level. The modern bioclimate at Fumane is humid and temperate continental (Rivas-Martínez et al. 2011), characterized by a mean annual temperature of c. 12.4°C, mean temperatures of the warmest and coldest months of 22.6°C and 1.5°C, respectively, and a mean annual precipitation (MAP) of 827 mm as derived from climate normals of the meteorological station Verona-Villafranca (45°23' N, 10°52' E, 68 m asl) situated 23 km south of Fumane Cave (Blasi et al. 2007; López-García et al. 2015). Regarding the paleoclimate conditions during MIS 3–2, several geological climate archives of the wider area (for locations, see Figure 1) indicate phases of cold and dry conditions

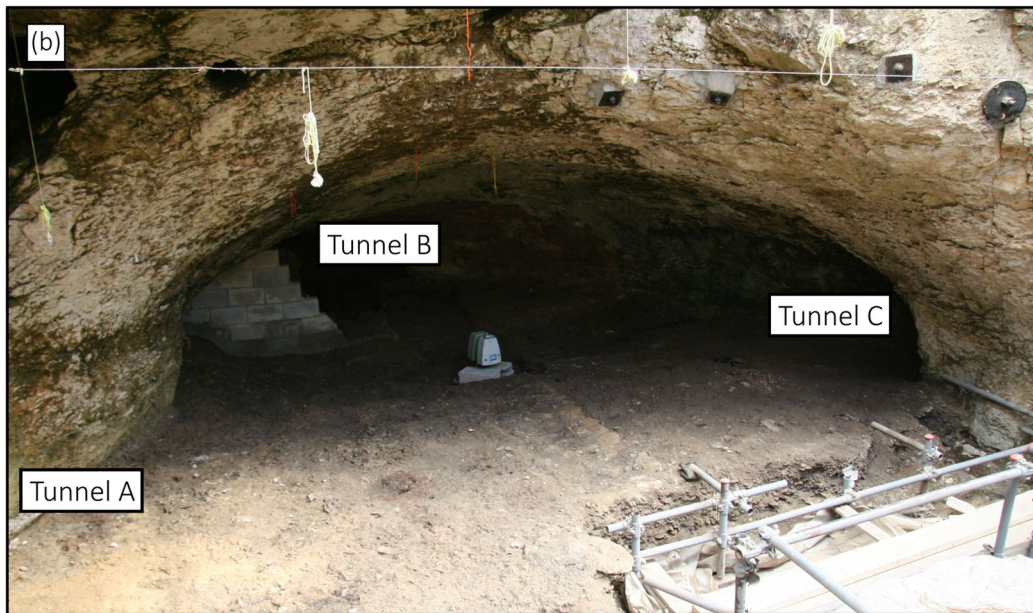
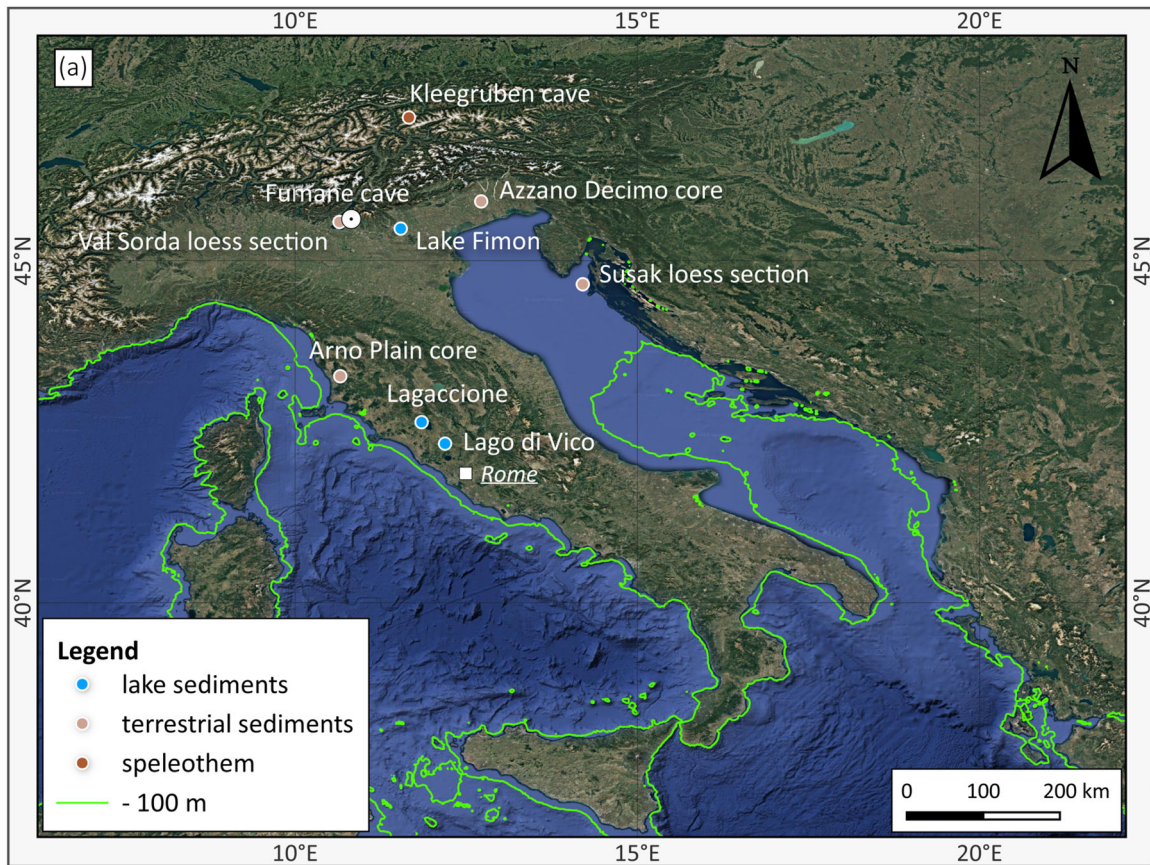


FIGURE 1 | (a) Location of the Fumane Cave and of the main sedimentary climate archives in Italy and the Alps mentioned in the text. The -100 m isobath indicates that, during the Last Glacial, the land mass in the Po plain extended further toward the southeast, causing a more continental climatological setting. (b) Image showing the cave entrance in 2013 during geophysical prospections with the location of tunnels A, B, and C.

such as limnic sediments of Lake Fimon (Pini et al. 2010; Badino et al. 2023), the Azzano Decimo core in the Po Plain (Pini et al. 2009; Badino et al. 2020), and sediment cores from Lago di Vico and Lagaccione (Voelker 2002) and from the Arno coastal plain (Aguzzi et al. 2007). Further evidence of dry and cold climate is provided by intensified dust accumulation in Val Sorda in the Garda Lake morainic amphitheater (Ferraro 2009) and on

Susak Isle (e.g., Wacha and Frechen 2011). Dansgaard-Oeschger climate cyclicity during MIS 3 (Dansgaard et al. 1993) is reflected, for instance, in speleothems from Klee gruben cave (e.g., Spötl et al. 2006).

The cave consists of several smaller cavities and a karst pit developed in yellowish to reddish, poorly stratified, and weakly

inclined Jurassic dolostone and dolomitic limestone. Three tunnels open at the upper levels of the karst complex (Figure 1). The main (B) and secondary (C) tunnels form the major rock shelter, whereas a third western (A) tunnel connects with B, forming a vault at the present-day cave entrance in the dolostone bank, still unstable due to several fractures running roughly parallel along the overhung rock wall. These cracks are a consequence of collapse events that caused the sealing of the cave entrance and the deposition of large blocks and slabs. Hence, the cave entrance was originally positioned a few meters south than the present. Today, the sheltered entrance is about 30 sqm large. The cavities are filled by unconsolidated, sandy, and stony deposits forming a sedimentary sequence, about 12 m thick. The sequence was divided into four macro-units based on sedimentological and pedological features as well as the density of archaeological finds (Cremaschi et al. 2005). The lowermost macro-unit S consists of residual dolomitic sands, probably re-worked by fluvial action with inclusions of partially weathered boulders from the cave roof and of some levels indicating living floors. Macro-unit BR comprises breccia with a matrix of eolian silt and clay. Archaeological finds of Mousterian affinity are mainly dispersed, but a thick living floor in BR11 is found as well. The next macro-unit A (Figure 2) contains several horizontally layered units (A13–A1) consisting of residual sands, locally disturbed by frost heaving (A13–A12), cryoclastic breccia, and a fine-grained matrix of eolian silts. In comparison to macro-unit BR, macro-unit A shows much more evidence of human occupation, including several living floors with sediment features resembling hearths. Macro-unit A records the MP/UP transition with Mousterian occupations indicated in units A11, A10, A9, A6–A5, and A4 (Peresani 2012, 2022), the Uluzzian technocomplex represented in A3 (Peresani et al. 2016), and the Proto-Aurignacian contexts in A2 and A1 and D3 (Falcucci et al. 2017, 2024). These units were extensively excavated at the cave entrance down to unit A10. Units A13, A12, and A7 are archaeologically sterile. Macro-unit D at the top of the sequence is composed of large roof-fall blocks probably related to intense frost activity. Human presence becomes sporadic and ends with the Gravettian subunit D1d (Falcucci and Peresani 2019).

The sequence from the MP to UP probably spans the period from MIS 7 to MIS 2 (Falgüeres, pers. comm.; Peresani et al. 2022). Higham et al. (2009) discussed radiocarbon dates from the Gravettian to late Mousterian units (D1e to A11), suggesting that the main factor causing dispersion of dates is contamination. This is demonstrated by the re-dating of charcoal from the Aurignacian, Uluzzian, and Mousterian units D3 to A5, previously dated using conventional pretreatment and now subjected to rigorous pretreatment to eliminate contamination applying the ABOx technique (Higham et al. 2009). This procedure yielded considerably older ages pointing to age underestimation by conventional pretreatment protocols. Additional radiocarbon measurements on bone for Uluzzian unit A3 and now reassessed Mousterian unit A4 yielded ages between 39 and 42 ka (Douka et al. 2014, Marín-Arroyo et al. 2023). These partially overlap with radiocarbon dates for the Mousterian units A5 and A6 (Higham et al. 2009, 2011). Mousterian unit A9 is chronologically not well constrained and probably underestimated by published radiocarbon dates (see fig. 7 in Badino et al. 2023), but a correlation with a relatively warm and

humid phase before Heinrich Stadial (HS) 5 was proposed (López-García et al. 2015). For comparison between climate signals of the Fumane sequence with regional climate records, the results of Bayesian modeling using 23 radiocarbon dates from units A5+A6, A4, A3, A1/A2, and D3 of the Fumane sequence as described in Marín-Arroyo et al. (2023) can be used as a chronological framework.

3 | Materials and Methods

3.1 | Field Description

The definition and description of stratigraphic units were carried out on both fresh exposures and undisturbed samples taken during the archaeological excavations from 1988 to 2019 (Bartolomei et al. 1992; Cremaschi et al. 2005; Peresani et al. 2008; 2011, 2017) following allostratigraphic and lithologic criteria (North American Commission on Stratigraphic Nomenclature 2005). The main features taken into account are the stratigraphic layout, architecture, lithological features (stoniness, coarse-fine fraction relation, fabric, structure etc.), boundaries, and indications of anthropogenic activity as shown by variable darkening of sediment due to organic content, lithics, bones, and charred vegetational residues. The micro-sequence in each sedimentary unit does not have a uniform pattern, although most of the units cover the entire cave's surface. Some discontinuities affect the whole sedimentary body or sometimes are restricted to a few units: lines of marmot burrows and gaps with irregular boundaries. Part of these features were already illustrated in previous studies (Bartolomei et al. 1992; Cremaschi et al. 2005; Peresani et al. 2011), whereas major parts of the descriptions remained unpublished in the last 25 years. Features are resumed here from the field notes taken after the examination of samples at eye scale and using 10X lens following Goldberg and Macphail (2006). Sediment color was recorded using Munsell Soil Color Charts (Munsell Color 2009).

3.2 | Sampling of Thin Sections and Micromorphological Techniques

Sediment monoliths for the preparation of thin sections were extracted from units D1, D3, and A1–A7 as well as A9–A11 from the entrance area (rows 4–6 of the excavation grid, Figure 3), the central part (rows 7–9), and the back part of the shelter (rows 10–14) in the course of excavation campaigns between 1999 and 2016 (Figure 3). For further information on thin-section origin, refer to Supporting Information S1: Tables S2 and S2.1. All thin sections from units A9 and above were prepared by Servizi per la Geologia Facility, Piombino, Italy, whereas thin sections from units A10 and A11 were produced in the Geoarchaeology Laboratory of Tübingen University, Germany, and by the Terrascope Thin Section Slides laboratory, in Troyes, France. Further details on sampling are provided in the supplementary materials.

Most of the observations were made on thin sections from columns 9–7 and rows 5–9 of the excavation grid (Figure 3). This sample collection bias has to be considered when

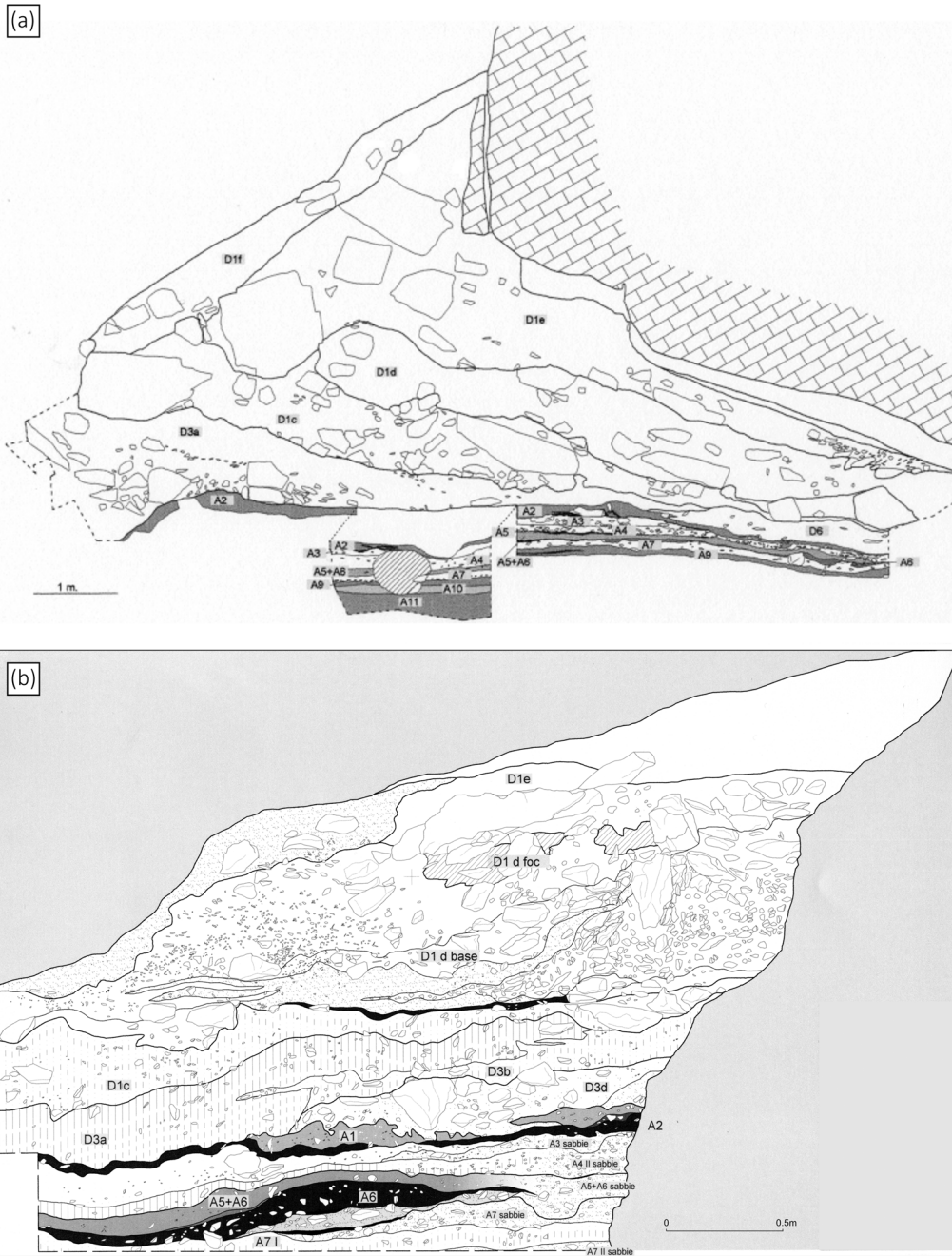


FIGURE 2 | (a) Upper part of the main sagittal section now partly dismantled at the cave entrance, with the main lithological features in D and A macro-units and sequence of stratigraphic units from A11 to D1. (b) Stratigraphic sequence from A7 to D1 visible on the section at the entrance of tunnel A with evidence of late Mousterian (A6–A5, A4), Uluzzian (A3), Aurignacian (A2–D3), and Gravettian (D1) units. Note the wavy deformation of units A1 and A2. The degree of anthropogenic content is represented by progressive darkening from white (very low/absent) to dark gray/black (very high).

interpreting the spatial distribution of sedimentary properties observed in thin sections across the excavated area.

The thin sections were studied using a polarizing microscope and flatbed scans. For micromorphological description, the system and terminology of Stoops (2021) were followed. The properties of groundmass and pedofeatures (see the Supporting Information for further explanations) were observed at different scales under plane polarized light (PPL) or crossed polarizers (XPL). In a few cases, micrographs were captured under circular polarized light (see figure captions). Oblique

incident light (OIL) was used to distinguish opaque components according to tab. 3.2 of Stoops (2021). Quantitative criteria used for the description are listed in Supporting Information S1: Table S2.2. For quantitative estimates of the surface area covered by coarse components and voids, reference charts (Stoops 2021, fig. 4.12) were used. The abundance of silt cappings in each unit was quantified by calculating a weighted mean of the number of observations in each abundance class. The resulting cappings index can range from 0 for absence of cappings to 1 for abundance class "many" in all observations for a certain sedimentary unit.

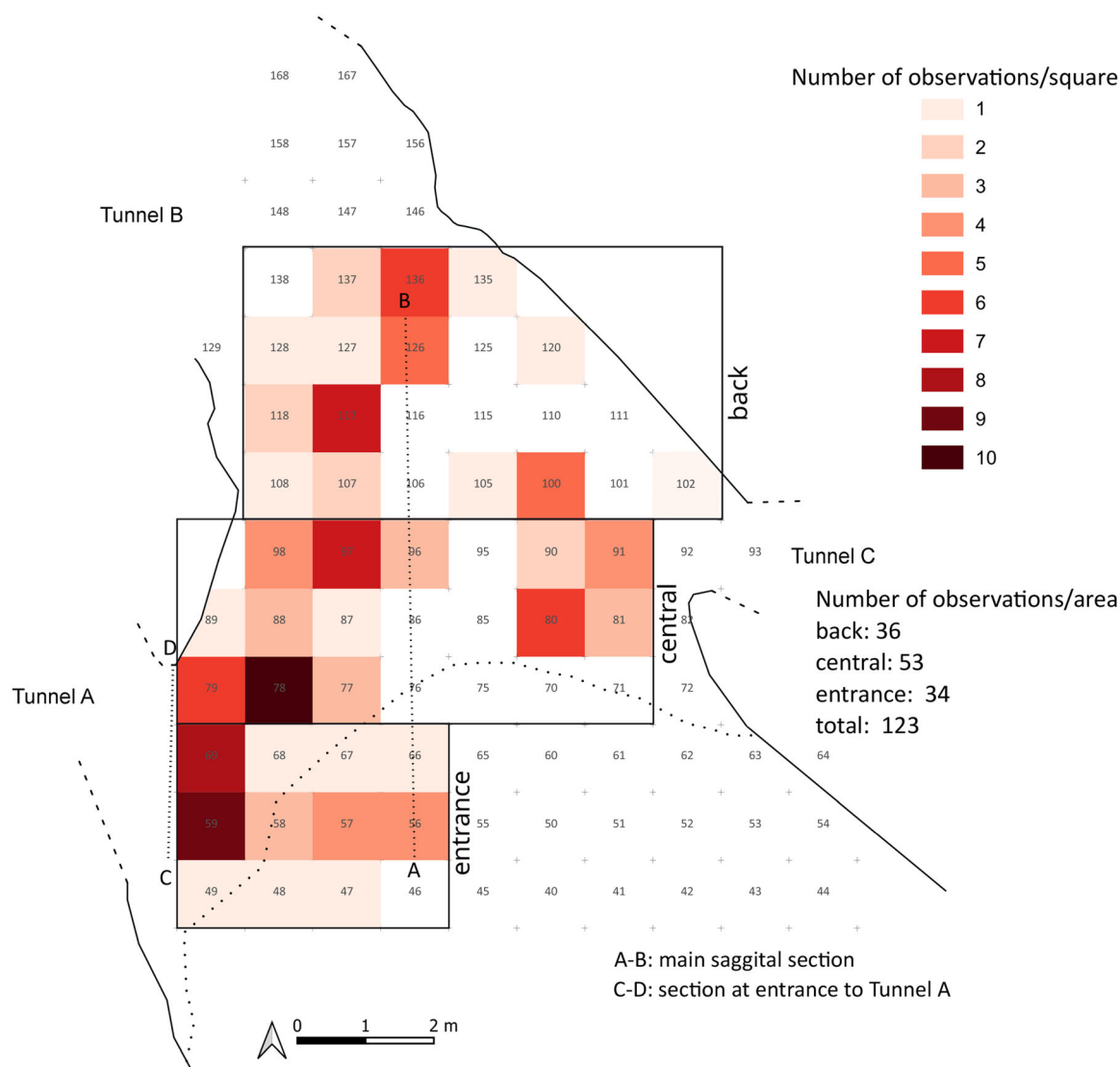


FIGURE 3 | Number of micromorphological data sets ($n = 123$) for all subunits identified in thin section as plotted on each square meter of the excavation grid. The thin sections mainly derive from the left-hand side of the central cave and the entrance area, whereas comparatively few are available from the outer part of the entrance area and the right-hand side of the excavation grid.

4 | Results

4.1 | Field Description of Stratigraphic Units D1 to A13

The deposits of macro-unit A, labeled A13 to A1 from bottom to top, mostly consist of numerous thin parallel layers and horizontally bedded lenses, grouped into stratigraphic units. The units of macro-unit D (from D3 to D1) have large thicknesses, show strong variation in their textural components, bend toward the inner cave, and ultimately seal the cave entrance. All stratigraphic units from D1 down to A13 extend over the whole cave entrance and the inner cave mouth and are currently exposed on several sections in the excavated sectors: at the entrance of tunnel A (from A9 to D1e); in the cave mouth in tunnel B (from A11 to A10 and A9 to D1e); in the present-day exterior area in the trench and pit opened in 1990 and 1992, respectively (from A13 to A3); and at the small entrance of tunnel C (from A10 to D6). Although detailed information on the sedimentary properties of each unit is provided in the Supporting Information S1:

Text and Figures S1.1–S1.18, a summary description is provided in Table 1. The thickness of sedimentary units ranges from less than 5 cm such as in the anthropogenic deposit D3alpha to 350 cm in subunit D1e–D1f. Most layers and lenses are characterized by frequent to dominant abundance of angular or sub-angular limestone clasts reaching boulder size in unit D1, whereas rock fragments of other units fall into size classes of small to large stones. Those layers and lenses show clast supported to openwork fabric. A few subunits such as A3l are comparatively poor in rock fragments. The texture of the fine fraction resembles sand, loamy sand, silty loam, and loam, reflecting increasing contents of silt and clay toward loams. A poorly to moderately developed granular aggregation is observed in some units. The interfaces between units are mostly characterized by abrupt boundaries, which, in the upper part of the sequence, often show deformations. Various contents of anthropogenic components reflect diachronic changes between dominantly natural and anthropogenic sediments, the latter characterized by increased organic content and abundances of lithics, bones, and charred vegetational remains. Concerning

TABLE 1 | Field description of the Fumane Cave sedimentary sequence.

Unit	Subunit	Sedimentary unit layout	Thickness (cm)	Lower boundary	Coarse fraction	Fine fraction	Munsell color	Sorting	General structure	Aggregation	Anthropogenic degree	Facies	Notes
D1	D1e-D1f	Thick layer	40	Abrupt with deformations	B, LsS	LS	—	Poorly sorted	Angular clasts with parallel long axes to depositional surfaces	—	Carnivore den	Rubble; Top soil (rendzina) in D1f.	
	D1d	Thick layer	40–90	Abrupt	B, LsS	SL	—	Poorly sorted	Angular platy clasts (****)	—	Weak	Rubble	Includes D1dbase
	D1c	Thick layer	30–90	Abrupt with deformations	B	S	Not determinable			—	—	Rubble	
D3	D3a-D3b	Layer	<30	Clear	SsS	LS	10YR3/4-6	Well sorted	Angular platy clasts parallel to depositional surfaces	MD, FGr	Moderate	Rubble	
	D3balpha	Thin layer	<5	Clear	MsS-LsS	SL	10YR4/3	—	Sandy strips intertwined with dark sediments	—	Intense	Anthropogenic	Anthropogenic features
	D3a+b sabbie	Layer	<15	Abrupt	—	S	—	Sorted	Sandy strip	—	—	—	Above A2 and A2R includes D3 + D6
	D6	Thick layer	<80	Abrupt	MsS	LS	Not determinable	Sorted	CS; angular platy clasts	—	Weak	Rubble	
	D3d	Thick layer	20–40	Abrupt with deformations	LsS	LS	Not determinable	Poorly sorted	B; subangular platy clasts (****)	—	Moderate	Rubble	
	D7	Layer	40	Abrupt	LsS	—	Not determinable	Poorly sorted	—	—	—	Rubble	
	D5	Layer		Abrupt	LsS	LS	Not determinable	Poorly sorted	—	—	—	Rubble	Includes D4 (rubble)
A1	A1	Thin layer	<5	Clear with deformations	—	SL	10YR3/2	Poorly sorted	Angular platy clasts (***)	PD, FGr	Intense	Anthropogenic	A1 alpha (rubble) Anthropogenic features
A2	A2	Layer	10–15	Abrupt with deformations	MsS	SL	10YR2/1	Poorly sorted	Angular-subangular platy clasts (***) parallel to depositional surfaces	PD, FGr	Intense	Anthropogenic	Anthropogenic features
	A2R	Layer	~10	Abrupt with deformations	MsS-LsS	L	7.5YR6/4	Sorted	Angular-subangular platy clasts (****) parallel to the depositional surfaces	—	Moderate	Rubble	Other coatings

(Continues)

TABLE 1 | (Continued)

Unit	Subunit	Sedimentary unit layout	Thickness (cm)	Lower boundary	Coarse fraction	Fine fraction	Munsell color	Sorting	General structure	Aggregation	Anthropogenic degree	Facies	Notes
A3	A3	Thin layer	~10	Clear with deformations	M _{SS} -L _{SS}	SL	—	Poorly sorted	CS; angular-subangular platy clasts	—	Moderate	Rubble	Anthropogenic features
	A3I	Thin layer	~8	Clear with deformations	M _{SS} -L _{SS}	L	10YR5/4	—	CS; A-SA platy clasts	—	—	—	Intrusive Aurignacian (A2) content
	A3II	Thin layer	~8	Clear with deformations	M _{SS} -L _{SS}	L	10YR5/3	—	D; A-SA platy clasts chaotically dispersed	—	—	—	Intrusive Aurignacian (A2) and Mousterian content
	A3s	Lens	~5	Abrupt	—	S	—	—	—	—	—	—	—
	A3I	Layer	~15	Clear	—	L	—	—	—	MD, FGr	Weak	—	—
A4	A4	Thin layers and lenses	10	Abrupt with deformations	S _{SS} -M _{SS}	LS	10YR6-5/4	Poorly sorted	Angular platy clasts (**/*****) chaotically dispersed	PD, FGr	Moderate to Weak	Rubble	Includes A4I, A4III Anthropogenic features
A5 and A6	A5	Aggradation of layers and thin layers	~25	Abrupt with deformations	M _{SS} -L _{SS}	SL	—	Sorted	Angular platy clasts (*****)	PD, FGr	Intense	Rubble	—
	A5	Thin layer	< 5	Abrupt	M _{SS} -L _{SS}	SL	10YR4/2	—	Angular platy clasts (***)	—	Moderate	Anthropogenic	Anthropogenic features
	A5BR	Stone level	5	Abrupt	M _{SS}	—	—	Sorted	CS; angular platy clasts parallel to depositional surfaces	—	—	Rubble	—
	A5 + A6	Layer	10	Abrupt	M _{SS} -L _{SS}	LS (lenses)	10YR3/2	Poorly sorted	Angular platy clasts (*****)	—	—	Rubble	A5+A6reccialII Anthropogenic features
	A5+A6sabbie	Lens	5	Abrupt	—	S	10YR5/6	Sorted	—	—	—	—	—
	A6	Layer	10	Abrupt	M _{SS}	LS	10YR3/4	Poorly sorted	Angular-subangular platy clasts (****)	MD, FGr	Intense	Anthropogenic	Includes lenses A6breccia, A6sabbie Anthropogenic features
A7	A7	Layer	~20	Abrupt	M _{SS} -L _{SS}	SL	10YR5-6/6	Sorted	CS; angular-subangular	—	—	Rubble	Intrusive anthropogenic

(Continues)

TABLE 1 | (Continued)

Unit	Subunit	Sedimentary unit layout	Thickness (cm)	Lower boundary	Coarse fraction	Fine fraction	Munsell color	Sorting	General structure	Aggregation	Anthropogenic degree	Facies	Notes
A7	A7sabbieI	Lens	15	Abrupt	—	S	10YR6/6	Sorted	platy clasts; speleothems fragments (*)	—	—	—	content (A6–A9)
	A7sabbieII	Lens	5	Abrupt	—	S	10YR6/6	Sorted	—	—	—	—	—
A9	A9sabbieI	Aggradation of thin layers and lenses	< 20–30	Abrupt with deformations to A10	MsS-LsS	SL	10YR3/2	Sorted and poorly sorted	Angular-subangular platy clasts (***)	PD, FGr	Intense > to bottom	Rubble	Incipient soil
	A9sabbie0	Lens	5	Abrupt	—	S	10YR5/6	Sorted	—	—	—	—	—
A9I	A9I	Thin layer	> 5	Abrupt	SsS-MsS	SL	10YR3/2	Sorted	—	PD, FGr	Intense	Anthropogenic	Anthropogenic features
	A9sabbieI	Lens	> 5	Abrupt	—	S	10YR5/6	Sorted	—	—	—	—	—
A9BRI	A9BRI	Thin layer	> 5	Abrupt	SsS-MsS	SL	10YR3/2	Sorted	—	PD, FGr	Intense	Anthropogenic	Anthropogenic features
	A9sabbieII	Lens	> 5	Abrupt	—	S	10YR5/6	Sorted	—	—	—	—	—
A9BRI	A9BRI	Lens	10–30	Abrupt	MsS-LsS	—	Not determinable	Sorted	OW; clasts parallel to depositional surfaces	—	—	Rubble	—
	A9II	Thin layer	> 5	Abrupt	SsS-MsS	SL	10YR3/2	Sorted	—	PD, FGr	Intense	Anthropogenic	Anthropogenic features
A10	A9BR	Lens	20	Abrupt	MsS	—	Not determinable	Sorted	OW; angular platy clasts	—	—	—	—
	A10I	Aggradation of layers and thin layers	~30	Abrupt	MsS-LsS	SL	10YR3/2	Poorly sorted	Angular-subangular lar platy clasts (****)	PD, FGr	Moderate to Intense	Rubble	Anthropogenic features
A10II	A10I	Thin layers and lenses	< 8	Abrupt	MsS-LsS	L	10YR3/2	Sorted	CS; angular-subangular platy clasts parallel to depositional surfaces; carbonate L	—	Moderate	Rubble	A10IBRI, A10IBRII, A10I.2, A10I.1 Anthropogenic features
	A10II	Thin layer	< 8	Abrupt	LsS	L	10YR5/6	Sorted	CS; rubble; angular-subangular platy clasts (****)	PD, FGr	Moderate to intense	Anthropogenic	A10IIL1, A10IIL1, A10IIBRIII Anthropogenic features
A10IV	Thin layer	< 5	Abrupt	SsS	CL	10YR4/3	Sorted	CS; angular-subangular platy clasts parallel to depositional surfaces	MD, FGr	Intense	Anthropogenic	A10IV.I Anthropogenic features	

(Continues)

TABLE 1 | (Continued)

Unit	Subunit	Sedimentary unit layout	Thickness (cm)	Lower boundary	Coarse fraction	Fine fraction	Munsell color	Sorting	General structure	Aggregation	Anthropogenic degree	Facies	Notes
	A10V	Thin layer	<8	Abrupt	M _s S	SL	10YR5/4	—	to depositional surfaces angular-subangular platy clasts parallel to depositional surfaces	—	—	Rubble	A10V_BRIV
A11		Layer	~10	Abrupt	M _s S	LS	10YR3/2	Poorly sorted	D, SA platy clasts, mostly parallel to depositional surfaces	PD, FGr	Intense	Anthropogenic	A11a-d, A11base
A12		Layer	<10	Abrupt with deformations	M _s S	SL	10YR5/6	Poorly sorted	Subangular platy clasts (***) vertical.	—	Intrusive	Rubble	
A13		Layer	<10	Abrupt	M _s S	S	10YR4/6	Poorly sorted	CS	—	—	Rubble	

Note: Sabbie = sand. The Munsell color is ascribed to moist sediment. Key: Abundance: very few: *, few: **, common: ***, frequent: ****, dominant: *****. Degree of pedality: PD, poorly developed; MD, moderately developed; SD, strongly developed. Structure: CS, clast supported; MS, matrix supported; OW, openwork. Texture fine fraction: SL, silty loam; LS, loamy sand; S, sand; L, loam; C, clay. Texture coarse fraction: B, boulders; L_sS, large-size stones; M_sS, medium-size stones; S_sS, small-size stones. Aggregation: FGr, fine granular. Anthropogenic degrees: weak: natural sediment with very sparse lithics and anthropogenically modified bones; moderate: natural sediment with scattered anthropogenically modified bones, lithics, charcoal, and sparse fireplaces; and intense: dark sediment, with abundant charcoal, fireplaces, and densely distributed lithics and anthropogenically modified bones.

some Mousterian and Protoaurignacian contexts, especially A9, A6, and A2, macroscopic evidence confirms a mainly anthropogenic origin of the remains and sediment features, whereas in units A5, A4, A3, and D3, anthropogenic sedimentation is relatively sparse or differentiated. In rare cases, such as in units A7 and partly in A3, anthropogenic features intruded from overlying anthropogenic deposits.

4.2 | Micromorphological Features

In the following, a general description of the mineral and organic components and the fabric of the sediments as seen under the microscope is provided.

4.2.1 | Mineral and Organic Constituents

Rock fragments of dolomitized limestone and tufa, mostly showing flat, angular, or subangular and rarely rounded shape (Figure 4), dominate the coarse particle size fraction. Other rock types are rarely found. Field descriptions show that the long axis of elongated clasts is often oriented parallel to the former cave floor. This is reflected in the horizontal orientation of long axes in thin sections. Weakly inclined (max. angle of 5–10° to the horizontal, Figure 4a), oblique (around 45°), and vertical orientations were observed too. Often, different orientations were present in the same thin section (Figure 4b). Several limestone clasts show laminar calcareous coatings (Figure 4c), resembling laminar carbonate crusts forming on bedrock (Durand et al. 2018). There is no microscopic evidence that coatings were related to the accumulation of secondary calcite in the sediment itself. Few angular fragments of chert and flint represent by-products of tool production and are encountered in most sedimentary units (Figure 4e,f). Highly porous fragments of carbonate crusts resembling tufa (Supporting Information S1: Figure S2.1a,b) are rare. These have originally formed at the cave wall before dropping on the sediment surface.

The amount of limestone clasts varies to a large extent from less than 5% (e.g., Figure 4d) to very high (50%–70%, Figure 4c). There is a general tendency that thin sections from units D1, D3, and A10 are particularly rich in stones.

The fines (<2 mm in diameter) consist of silt and sand-size mineral grains as well as optically nonresolvable micromass (particles < ca. 5 μm). The grain size composition resembles pure sands, loamy sands, or sandy loam differentiated by increasing amounts of silt grains and micromass. Sediments resembling a loamy texture, that is, grain size distributions rich in silt and micromass were also found in anthropogenic sediment feature VI from unit A4 (Figures 4 and 5a–d). The loamy sand or sand dominates in most stratigraphic units, with the sand content being relatively high in units D1, A1, A3, A4, and A9, whereas sandy loams or loams are rarely covered in the thin-section sample (Supporting Information S1: Figure S2.2). The sand and loamy sand facies are most frequent in the left central part of the cave, whereas they were more rarely found in thin sections from the entrance area and the right-hand side of the cave (Figure 6). This partly reflects the evidence from the field, where sands were observed to prevail in the westernmost area at the entrance of tunnel A.

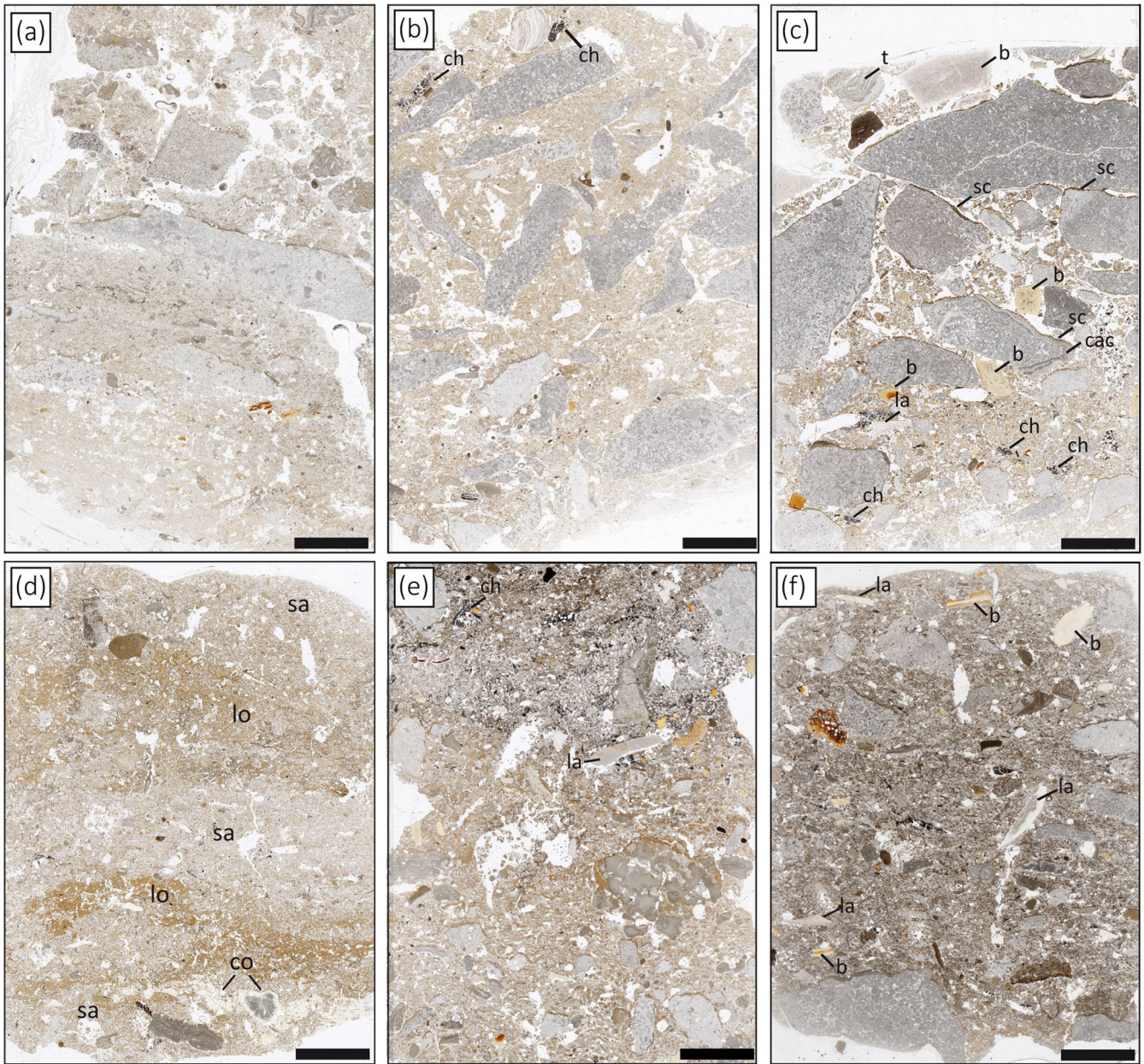


FIGURE 4 | Flatbed scans of selected thin sections from Fumane Cave (1200 dpi, captured using ordinary light in transmission mode, scale bars are equal to 10 mm). (a) Elongated frost-shattered dolostone fragments with a subhorizontal orientation of the long axis in a sandy groundmass. Note the compacted layer resulting from trampling underneath the rock fragment in the center (thin section A2 MS10). (b): Thin section MM3 from archaeologically sterile unit A7 with light-colored groundmass. Charcoal pieces at the top probably belong to the overlying unit A6. The long axes of elongated rubble do not show a preferential orientation. (c) Thin section A6 MM6 showing a high (50%–70%) proportion of limestone clasts and the presence of bone and charcoal fragments. The upper part of the thin section (unit A6) has a darker groundmass than the lowermost part (unit A7). Note the silt cappings on limestone fragments, partially superimposed on calcite coatings. (d) Thin section A4 MM8 from unit A4 feature VI shows intercalation of slightly loamy sand with loam (lo). Comparatively large pieces of coprolites are present in the lowermost sandy layer. (e) Sharp sedimentary boundary between dark-colored unit A1 at the top and the lighter colored unit A2 at the bottom (thin section A1 97d C2). (e) Dark sediment of unit A6 with a relatively high abundance of bone, small fragments of charcoal, and lithic artifacts (A6 MM42). Key: b, bone; cac, calcite coating; ch, charcoal; co, coprolite; la, lithic artifact; lo, loam; sa, sand; sc, silt capping; t, tufa.

The sand- and silt-size particles are mainly composed of carbonate grains, originating from the cave wall, whereas quartz and mica occur in subordinate amounts (Figure 5a–d). The siliceous components mostly belong to the coarse silt and fine sand fractions and show a good degree of sorting, which indicates that they could have entered the rock shelter by eolian transport.

Mostly small (< 2 mm in diameter) fragments of dense coprolites consisting of phosphate incorporating few carbonate and quartz grains are found in many thin sections (Figure 5e,f). Rarely, larger coprolites are preserved such as in thin section A6 MM6 within unit A6 (Figure 4d). The coprolites show vesicular and elongated pores, but inclusion of bone fragments, which would point to carnivore origin (Horwitz and Goldberg 1989; Brönnimann

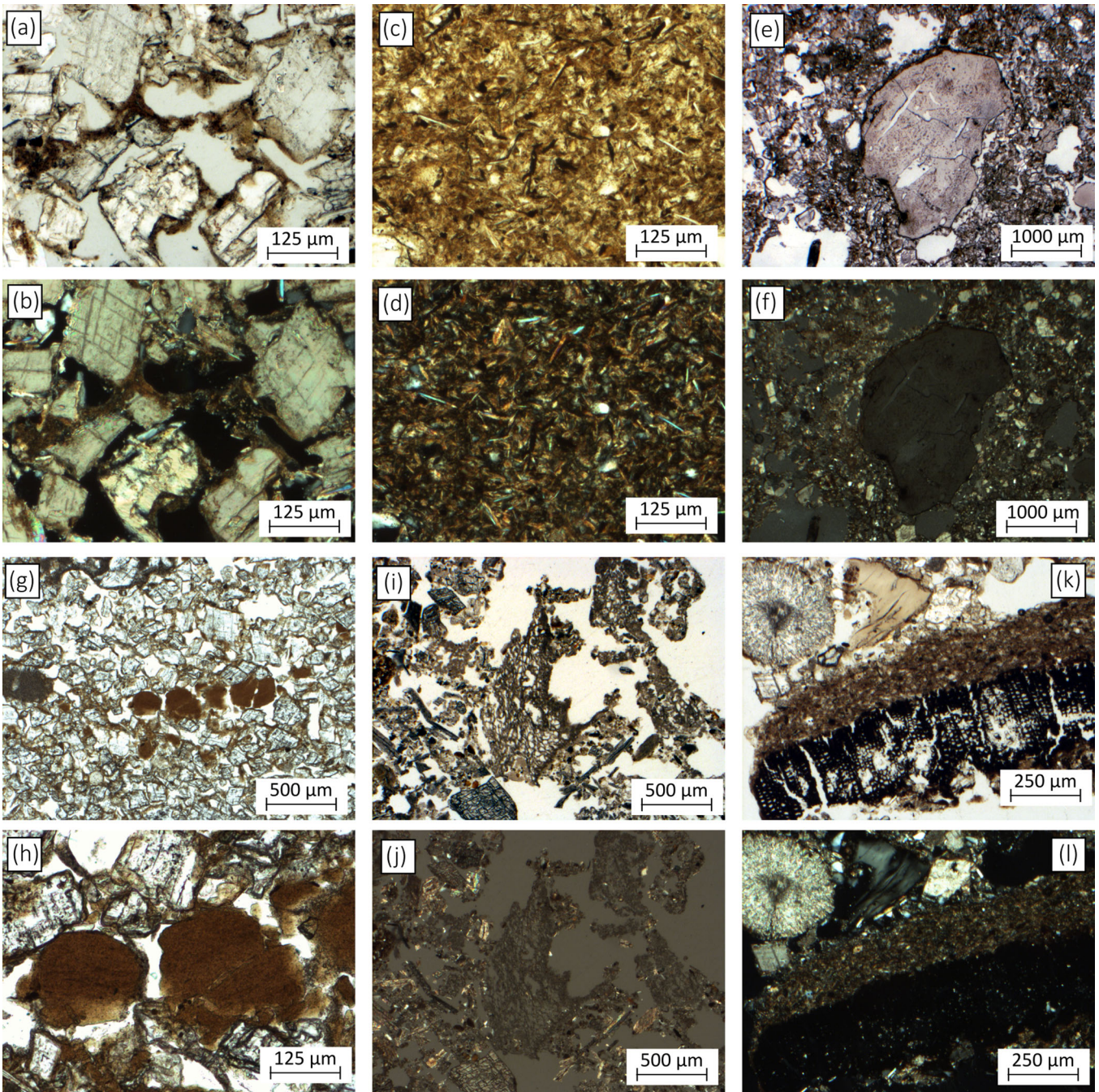


FIGURE 5 | Illustration of selected micromorphological features. A: Micrograph of sandy facies in thin section A4 MM8 from feature A4VI with fine to medium sand grains of calcite and a gefuric coarse/fine related distribution. (b) Same as (a) but captured under circular polarized light. Note the presence of few silt-size mica and quartz grains. (c, d) Micrographs of loamy facies in A4 MM8. (d) The presence of abundant mica grains is apparent under crossed polarizers. (e) Coprolite with elongated pores probably from fir hairs indicating a carnivore origin. (f) Same as (e) but under crossed polarizers. The isotropic phosphate of the coprolite appears in black. (g) Small accumulation of clay granules in thin section A7 MM2. (h) Some of the same clay granules as in (g) at higher magnification. (i) Remains of plant tissue (center), probably ashed (A9 MM4). (j) Same as (i) but crossed polarizers. (k) Piece of charcoal with cappings of silt and micromass. Note the calcite biospheroid in the upper left corner (A2 MS11). (l) Same as (k) but crossed polarizers. Key: b, bone; cac, calcite coating; ch, charcoal; co, coprolite; la, lithic artifact; lo, loam; sa, sand; sc, silt capping; t, tufa.

et al. 2017), was not observed. Short (< 5 mm) fragments of shell are present in traces in most thin sections. Longer fragments or even intact pieces of mollusk shells (Supporting Information S1: Figure S2.1c,d) were very rare.

Another interesting component is the presence of mainly sand size clay-rich silty aggregates interspersed in the carbonate

sands and locally aligned in discontinuous patches or bands (Figure 5g,h). Their circular shape points to transport and rounding in running water, while they may have endokarstic or exokarstic origin (Marcazzan et al. 2023).

Frequent constituents of organic origin are small (< 1 mm) to large (c. 10 mm) pieces of charcoal with well-preserved cell

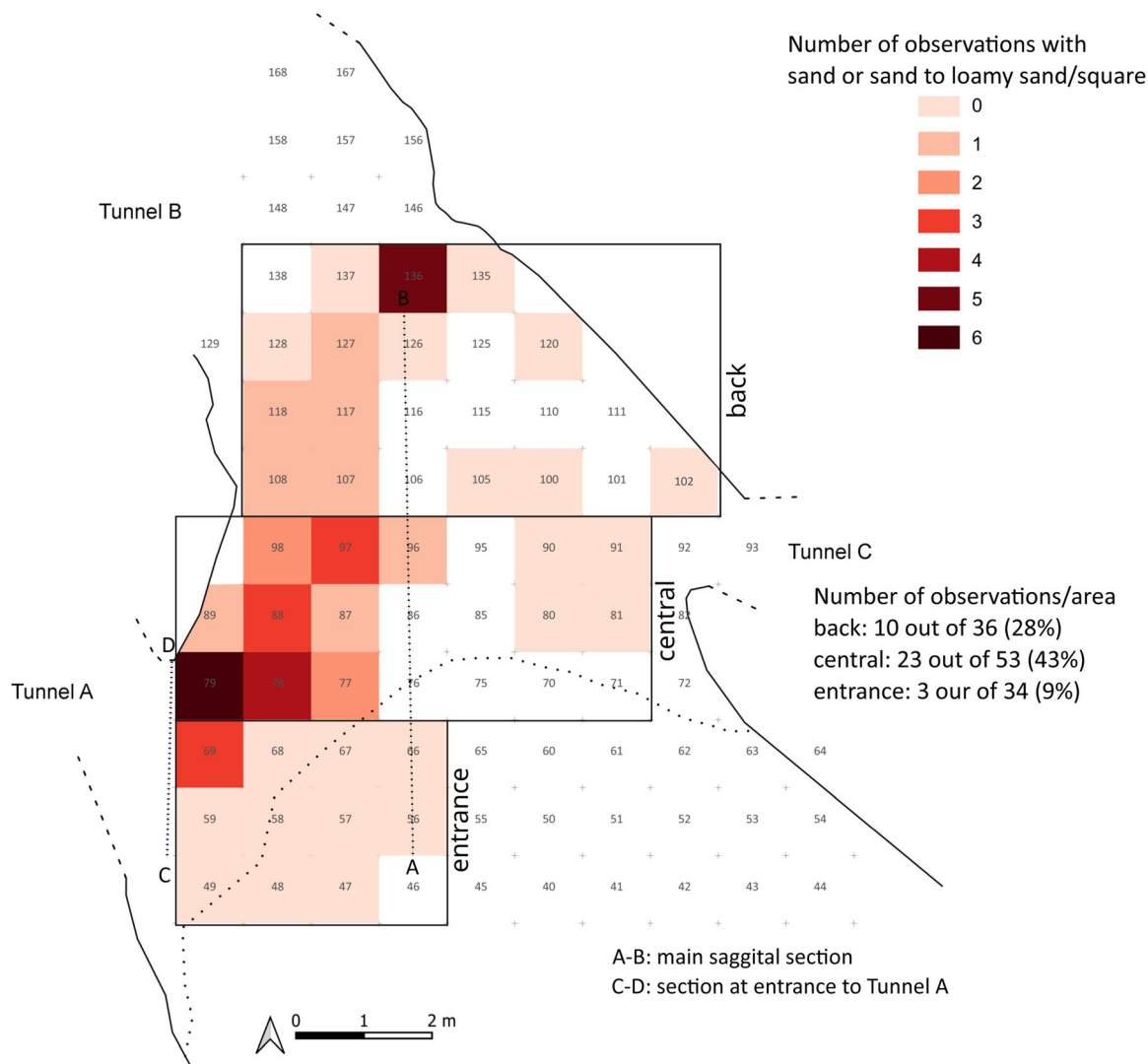


FIGURE 6 | Spatial distribution of sandy groundmass textures (sands and slightly loamy sands; $n = 36$) plotted on the excavation grid.

structures (Figures 4b,c,e and 5k,l). Besides charcoal, charred organic matter without recognizable cell structure is found in many thin sections. Char fragments are more abundant within anthropogenic features, where several pieces were identified as fat-derived char (Marcazzan et al. 2023, fig. 1f). Plant ash (e.g., Canti 2003) was detected in few thin sections, some of which originates from features (Marcazzan et al. 2023). The ash either occurs in distinct microlayers such as in features of unit A10 or as small clusters of ash particles in which plant structures are partly preserved (Figure 5i,j). Remnants of fresh plant material such as tissue of modern roots are very rare. Locally, very few biospheroids (Figure 5k,l) possibly originating from earthworms were detected.

Mostly well-preserved subangular to subrounded bone fragments (Figure 5c,f) are present in many thin sections. Bone color ranges from pale yellow gray over yellow orange to dark brown in PPL, with very dark interference colors under XPL. The typical ropy structure and birefringence colors (XPL) are often well preserved, but may be completely lost in burnt or calcined bone fragments, which were found in low numbers. The bone fragments visible in the thin sections are less than 15 mm long.

The abundance of anthropogenic materials, including charcoal, burnt matter, bone, and lithic artifacts per thin section layer, was estimated in three frequency classes, namely, very low contents (< 1%), low contents (1%–10%), and high contents (> 10%). Comparatively low abundances were found in units A3, A4, and A7, moderate abundances in D1, D3, A2R, and A5, and high abundances in A1, A2, A6, A9, and A10 (Supporting Information S1: Figure S2.3). The spatial distribution of samples rich in anthropogenic materials (> 10%) is plotted in Figure 7. Although the abundance of anthropogenic materials in column 9 is comparatively low, higher amounts were observed in thin sections from column 8. In general, most anthropogenic material detected under the microscope derives from the central part of the cave. Overall, the applied micromorphological approach did not identify clear hotspots of anthropogenic materials in the sampled area.

Another material of anthropogenic origin consists of ocher (Cavallo et al. 2017, 2018), which is abundant in subunit A2R (Figure 11), where it is finely dispersed, causing a reddish-brown color of the groundmass or of silt cappings under OIL. Rarely, sand-size fragments of ocher occur, mainly in thin

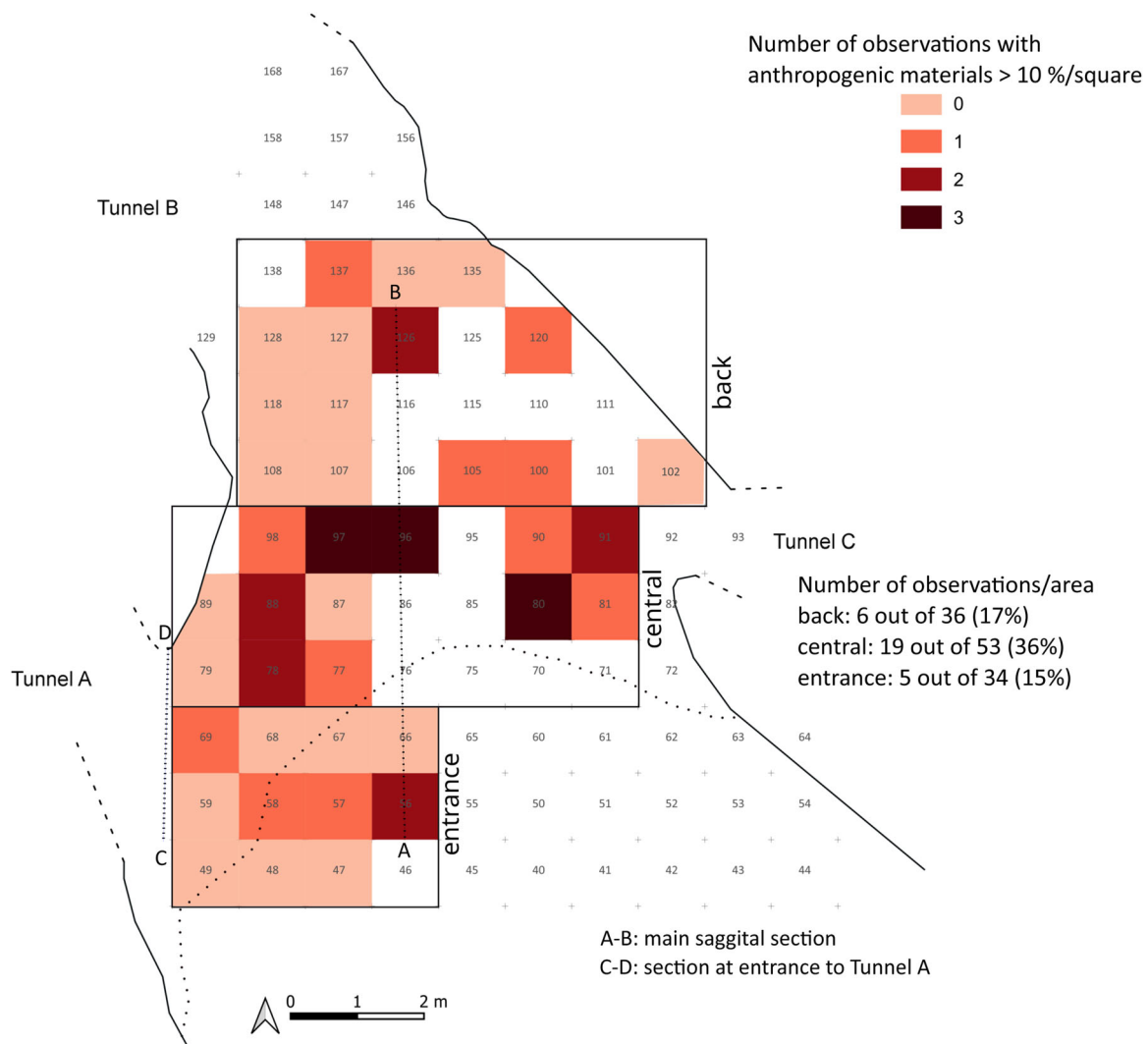


FIGURE 7 | Spatial distribution of samples comparatively rich in charcoal, charred organic matter, bone, and lithics regarded as anthropogenic materials ($n = 30$).

sections from unit A2. AS significant amounts of ocher were just found in thin sections from subunit A2R, it was not included in the estimation of anthropogenic materials.

4.2.2 | Basic Distribution Pattern, Voids, Aggregates, and Microstructure

Most thin sections show a random arrangement of components (e.g., Figure 8a,b). In a few cases, a banded fabric describing a preferential arrangement of coarse or fine grains in mostly discontinuous microlayers (Figure 8c,d,i,j) is expressed. The lateral shape of the bands is often bow-like and locally sinuous. Peresani et al. (2011) noted the presence of banded fabrics in unit A6 of the Fumane sequence, which is corroborated by this study. However, few thin sections from units A1, A2, A3, A4, A5, A6, and A7 show this fabric type (Supporting Information S1: Figure S2.4), which, overall, appears to be weakly expressed.

Clearly developed laminations indicative of low-energy deposition by sheet flow are not observed. Thin section A4 MM8

shows an interbedding of three sandy and three loamy layers (Figure 4d), suggesting different depositional regimes during accumulation. However, this thin section derives from a feature investigated by Marcazzan et al. (2023) and the bedding could be related to anthropogenic activities.

The porosity of the sediment ranges from low to extremely high, whereas most thin sections show a high or very high proportion of pores. Low porosities indicate higher degrees of compaction of mineral grains and organic materials as, for instance, observed in thin section MS10 from units A2/A3 in a thin layer, 2 cm thick (Figure 4a). The pore space in thin sections from sandy facies is often dominated by simple packing voids between individual mineral grains, resulting in single-grain microstructure (Figure 8a,b). In the case of higher silt and micromass contents such as in loamy sands, bridged-grain or pellicular microstructures are apparent (Figure 5a,b). Rarely, compound packing voids between non-accommodating aggregates (interaggregate voids) occur, where granules or sub-angular blocky peds are present. In a few cases, where small (< 3 mm in diameter) granules are present, a granular

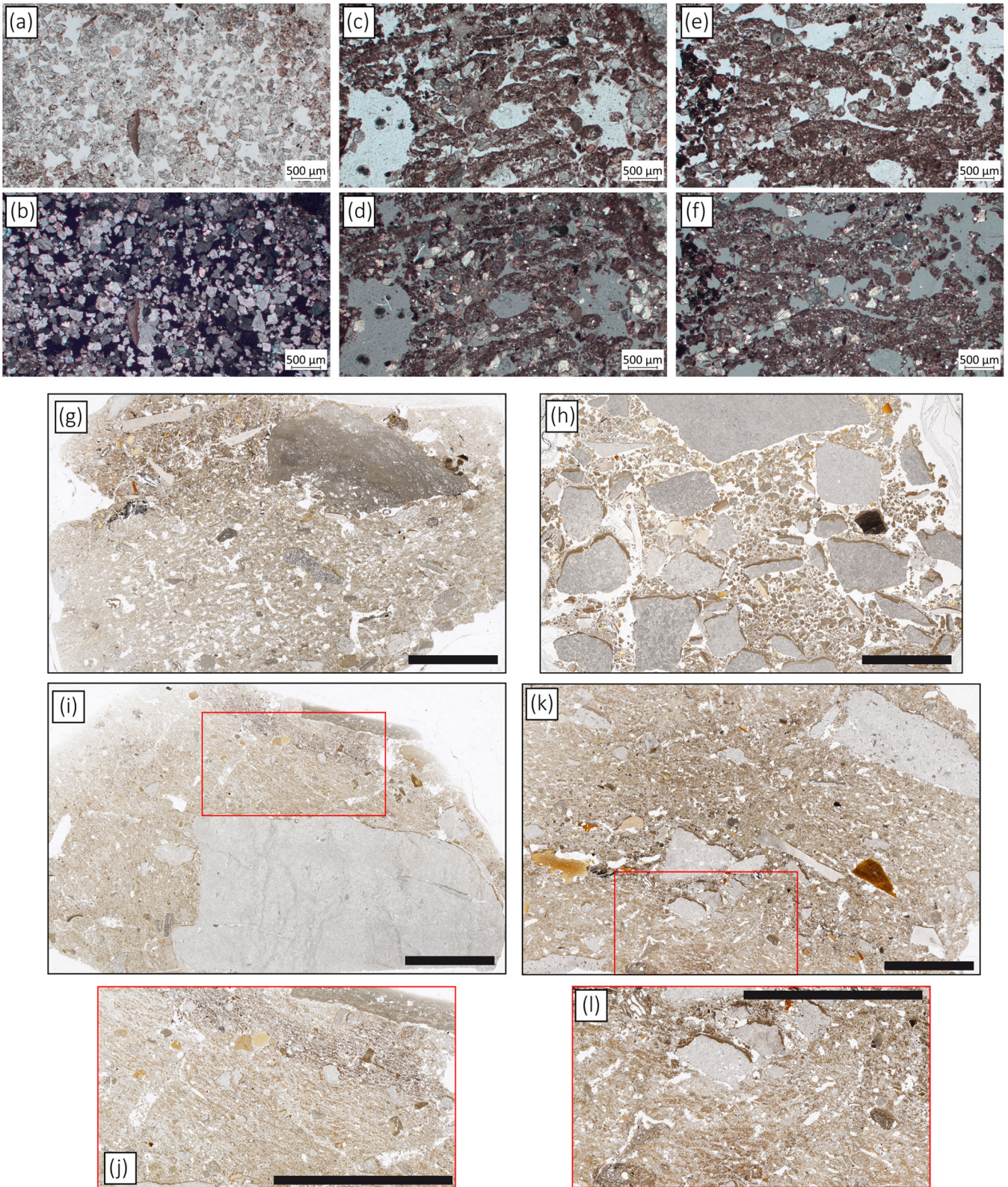


FIGURE 8 | Illustrations of microstructure and banded basic distribution pattern. (a, b) Coarse monic single-grain microstructure (A6 MM13) captured under PPL and XPL, respectively. (c, d) Weakly developed banded basic distribution pattern under PPL and partially crossed polarizers, respectively (A2 100h). (e, f) Lenticular aggregates, weakly developed and separated under PPL, and partially crossed polarizers, respectively (A2 100h). (g) Abundant channels and chambers in thin section A2 MM11 indicative of microscale bioturbation. (h) Well-expressed granular microstructure in thin section A10 16_17B. Note the prominent silt and micromass cappings on top of the limestone clasts. (i, j) Weakly developed banded fabric in thin section A4 MM7. (k, l) Weakly developed lenticular aggregates in A1_58c. Scale bars in flatbed scans equal 10 mm in length.

microstructure is expressed (Figure 8h). Vughy microstructure is found in massive (nonaggregated) groundmass with abundant vughs. Another very rare type of pores are planes between accommodating faces of aggregates of a very rarely expressed platy microstructure or cracks within limestone fragments. In a few thin sections with banded fabric, fine lenticular aggregates and a lenticular microstructure (Figure 8e,f,k,l) are present.

Biogenic pores, including burrows, channels, and chambers with smooth edges and circular to elongated round shapes, are present in many thin sections (e.g., Figures 4c–f and 8g). The channels often have diameters of < 1 mm. They can be several centimeter long when tangential or radial sections are visible. The size and high continuity of these pores indicate that fine plant roots induced their formation. The burrows and chambers are larger and more irregular in shape. If abundant, the microstructure is identified as burrow or chamber type. Their formation is related to soil-dwelling mesofauna (200–2000 µm in size) such as mites, springtails (Collembola), and insects, which feed on smaller animals and organic matter (Kooistra and Pulleman 2018). Locally, the burrows are incompletely filled with loosely packed granular organo-mineral aggregates, that is, excrements of soil mesofauna such as collemboles. Vughs with irregular shapes and partially rounded edges could represent former burrows that later deformed by settling processes. The frequent bio-pores suggest burrowing activity, which may have destroyed a formerly present ‘primary’ sedimentary structure. In some thin sections from features, the density of channels is particularly high in organic-rich layers. This may point to feeding of soil mesofauna on the organic materials probably shortly after the sediments were deposited. As the amount and type of pores can vary largely over the same thin section and sedimentary unit, different kinds of microstructures can be found next to each other. In addition, sandy and loamy microfacies in thin section A4 MM8 have clear upper and lower boundaries (Figure 4d). These characteristics indicate that bioturbation caused by soil mesofauna is restricted to the microscale.

4.2.3 | Coarse-to-Fine Related Distribution and Properties of the Micromass

We selected the threshold of 10 µm for distinguishing between coarse and fine grains. The coarse-to-fine ratio (c/f-ratio) thus ranged from about 60/40 in loam to > 95/5 in pure sand. The c/f-related distribution is classified as coarse monic in case of high c/f ratios, whereas close porphyric c/f-related distributions were observed in sediments showing higher contents of fines indicated by lower c/f ratios. If a preferential arrangement of fines in form of bridges between or coatings around sand grains is observed, a gefuric (bridges) or chitonic c/f-related distribution (coatings) is noted (Figure 5a,b). The latter type is commonly observed in sandy soil horizons with clay illuviation (argic horizons) (Kühn et al. 2018).

The micromass has a dotted limpidity and light brown to brown, reddish-brown, gray, or dark gray to black color, whereupon the color and optical properties of the micromass provide information on its mineralogical composition. The micromass contains micritic calcite, as indicated by a crystallitic

birefringence fabric (b-fabric) observed in most thin sections. If organic matter accumulation is high, the color changes to dark gray and an undifferentiated b-fabric results. Similarly, diffuse precipitation of secondary calcite and iron hydroxides influence groundmass color. A special case is the reddish-brown groundmass within thin sections from subunit A2R caused by finely dispersed ochre produced by anthropogenic activity (cf. Figure 11g,h). Finally, the micromass contains limited amounts of oriented silicate clay, very locally indicated by a weakly developed stipple-speckled b-fabric. Silicate clay is also included in sand-size orange-brown detrital granules of clay and silt (Figure 5g,h), as well as in coatings and cappings (see below). In many thin sections dominated by sandy detritus, the micromass is too few to allow further characterization.

4.2.4 | Pedofeatures

In thin sections from Fumane, frequent pedofeatures are related to the precipitation of secondary calcite forming typical nodules and diffuse impregnations of calcite, whereas calcite hypocoatings appear rarely. The nodules always have gradual boundaries toward the groundmass and often small channels are located within the nodules. Thus, transitional features between nodules, diffuse impregnations, and hypocoatings are often encountered. Incomplete micritic infillings and coatings in pores are rarely present. Few thin sections do not show any calcitic pedofeatures. Increased accumulation of secondary calcite is found in units D3, A1, A2, A3, and A4 (Figure 9). Moderate abundance of calcitic pedofeatures is observed in A5

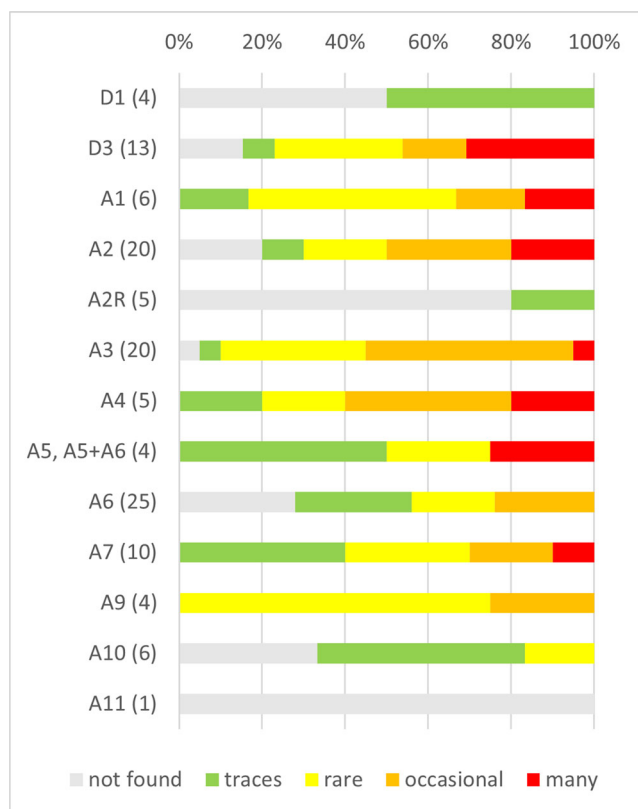


FIGURE 9 | Abundance rating of calcitic pedofeatures in different stratigraphic units.

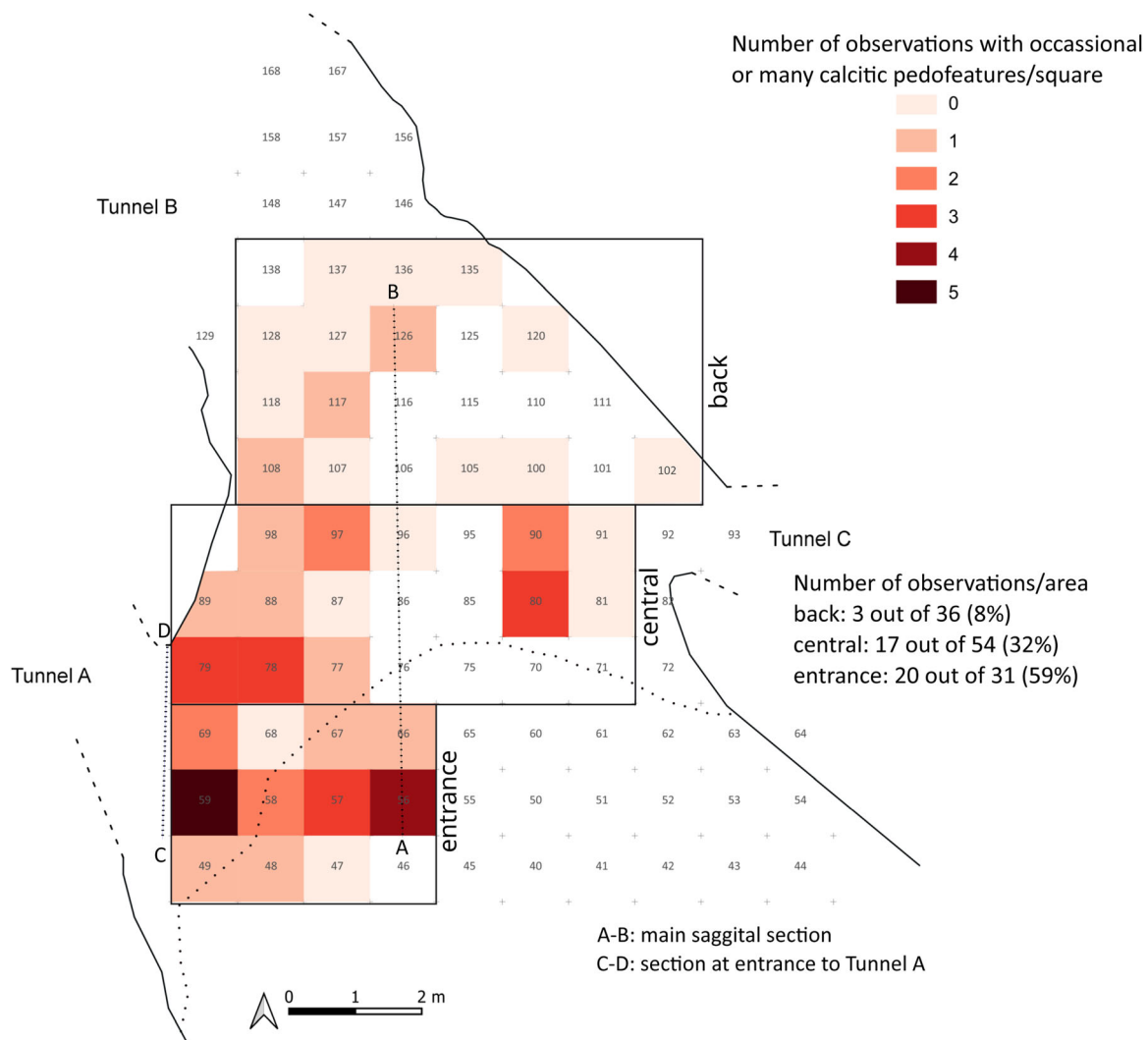


FIGURE 10 | Spatial distribution of thin sections with occasional or many calcitic pedofeatures indicative of high amounts of secondary carbonate ($n = 40$).

and A7, whereas rather limited frequencies are recorded for D1, A2R, A6, A9, and A10. As to the spatial distribution of calcitic pedofeatures, a high abundance is found near the entrance area in rows 5, 6, and 7 (Figure 10), whereas calcite precipitation was less pronounced in the back of the cave.

Silt-dominated cappings with inclusions of clay and sand particles (Figures 4c, 5k, and 11) are the most prominent textural pedofeatures at Fumane. Most of these so-called silt cappings (or silt droplets, Stoops 2021, 157) are thin to moderately thick (< 2 mm) and often discontinuous cappings on top of rock fragments or calcite coatings (Figure 11a,b). In very rare cases, similar features are present at the lower faces of fragments (Figure 11c,d). Within the silt cappings, elongated mineral grains are oriented parallel to the face of the rock fragments. Most of the silt cappings have light brown to brown color, whereas cappings of red or dark brown to black colors appear as well. The color of the silt cappings is clearly related to the color of the fines in the adjacent groundmass. This is documented in thin section A2 MM24, in which dark brown silt cappings occur in unit A2, reddish brown in subunit A2R, and light brown in

unit A3 (Figure 11h,g). In ash-rich layers of anthropogenic sediment features, silt cappings are dominated by ash particles (fig. 2J in Marcazzan et al. 2023). The close similarity of groundmass and cappings shows that the silt and clay traveled short distances before being filtered out on top of the surface. Cappings also occur on bone, charcoal (Figure 5k), or lithic fragments (Figure 11i) and in many thin sections, most upward-oriented faces are covered by them (Figure 8h).

The abundance of silt cappings is high in (sub)units A1, A2, and A2R as well as in A6 (Figure 12). Moderate abundances are recorded for thin sections from D3, A3, and A4, and rather limited numbers of cappings are present in units A5, A7, A9, and A10. No silt cappings were detected in thin sections from D1. Silt cappings occur in most sampled excavation squares, but there is a tendency for higher abundance in the central and back parts of the cave (Figure 13).

Another type of textural pedofeatures consists of dusty and impure clay coatings present in many thin sections (Supporting Information S1: Figure S2.5). These coatings are always thin

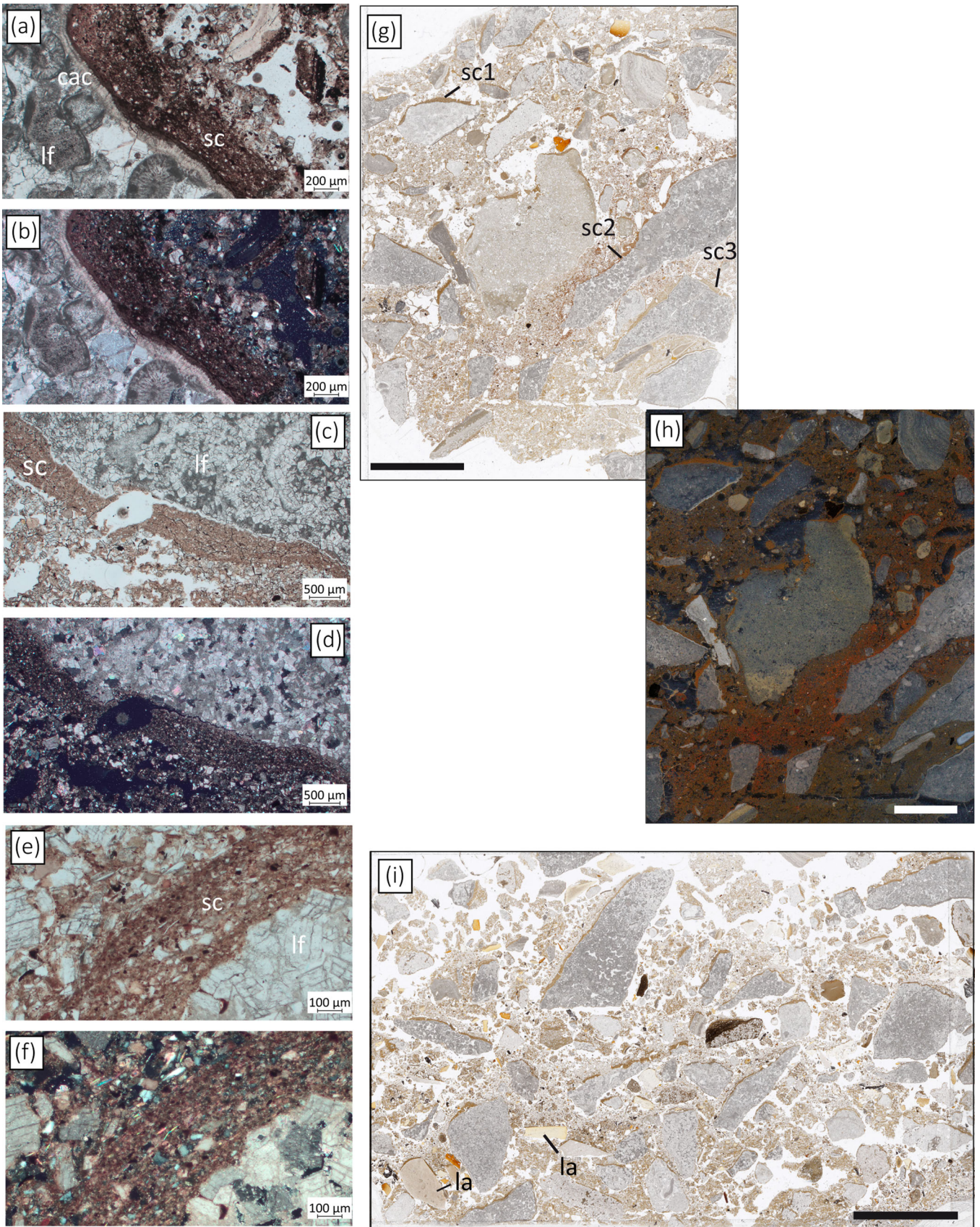


FIGURE 11 | Legend on next page.

(Supporting Information S1: Figure S2.1e,f) and mostly rare in abundance, whereas higher abundances were observed in combination with the expression of a gefuric or chitonic microstructure.

Pedofeatures other than those related to precipitation of secondary carbonate or silt and clay relocation are rare. Very few passage features are preserved. Secondary enrichment with phosphate is present in very few cases (Supporting Information S1: Figure S2.1g,h), a feature also described by Marcazzan et al. (2023). Redoximorphic pedofeatures such as nodules or coatings of manganese or iron were not observed.

4.3 | Weathering-Related Features

Few limestone fragments show dissolution hollows as signs of carbonate leaching (Figure 14a,b). Complete in situ physical disintegration into sand-sized dolomite crystals and formation of long fissures in limestone clasts are displayed in thin sections A6 MM13 and A7 MM2, respectively (Figure 14c–f). The sandy



FIGURE 12 | Relative abundance of silt cappings in different stratigraphic units.

FIGURE 11 | (a) Silt capping, ca. 500 μm thick on top of a thin calcite coating (< 100 μm thick) covering a limestone fragment (lf) in thin section A6 MM8. (b) Same as (a) but XPL. (c) Silt cappings at the lower face of a limestone fragment in thin section A6 MM13. This context occurs very rarely. (d) Same as (c) but XPL. (e) Silt capping in thin section A2 100 h. Note the regular arrangement of elongated mica grains. (f) Same as (e) but XPL. (g) Thin section A2 MM24 with brown silt cappings (sc1) on top of rock fragments in unit A2 (top), reddish brown (sc2) in subunit A2R (center), and thin light brown (sc3) in unit A3 (bottom). The different colors of the cappings indicate their local origin. (h) Reflected light scan and autocolor correction of Photoshop for part of the same thin sections showing the reddish color of subunit A2R. (i) Thin section A6 MM 2 with abundant thin silt cappings. Scale bars in flatbed scans equal 10 mm in length. Key: cac calcite coating, la lithic artifact, lf limestone fragment, and sc silt capping.

texture of many thin sections thus possibly derives also from mechanical disintegration in situ, which may have been enhanced by trampling on the cave floor.

Chemical and physical degradation of bone fragments appears to be weak. The dissolution of bone apatite or faunal phosphate nodules with later re-precipitation as infillings or impregnations of limestone fragments or within the groundmass was limited.

5 | Discussion

5.1 | Processes of Sediment Accumulation

The composition and fabric of different sediment layers at Fumane provide insights into major accumulation and alteration processes. The high abundance of subangular to angular dolostone gravel and larger clasts as well as the preponderance of sand or sandy loam textures in the fines (< 2 mm in diameter) consisting of carbonate mineral grains strongly suggest that deposition by gravity from the cave roof and wall (roof fall) was the major natural accumulation process in units A13–A1 (Figure 15). Elongated large blocks in macro-unit D are inclined parallel to the paleo-slope and appear to have been sliding into the cavity (Supporting Information S1: Figures S1.1a and S1.2c). It is thus likely that sediments of macro-unit D have accumulated by relatively slow processes of mass movement, including soil creep or solifluction in water-saturated sediment with or without effects of freeze–thaw cycles. The mass movement of D3d sediments affected unit A2, particularly in the easternmost internal zone of the cave entrance, where intrusions of A2 materials into D3d as well as an undulating interface between the two units were observed (Supporting Information S1: Figures S1.15 and S1.16). This was further confirmed by a blade break connection study. In particular, Falucci et al. (2024) conjoined several blade fragments recovered from D3d with fragments from the underlying unit A2. In contrast, orientation of elongated clasts in macro-unit A of the Fumane sequence is mostly parallel to the depositional surface, which is horizontal for these units (Table 1, Supporting Information S1: Figures S1.1 and S1.13), supporting the view of clast deposition by roof fall and lack of lateral transport. Vertical orientation of clasts in unit A12 is probably related to postdepositional reorientation. In thin section, grain orientation can be assessed in two dimensions; thus, the true orientation of particles is not known. In 2d, the long axes of elongated particles mostly show a horizontal orientation, but diagonal or vertical orientations are observed as well. Overall, the poor documentation of the first excavation campaigns (1989–1993), precludes any possibility of progress on fabric analyses. However, for sediments of A2 and below, it is thus very unlikely that mass movement was a significant process of deposition.

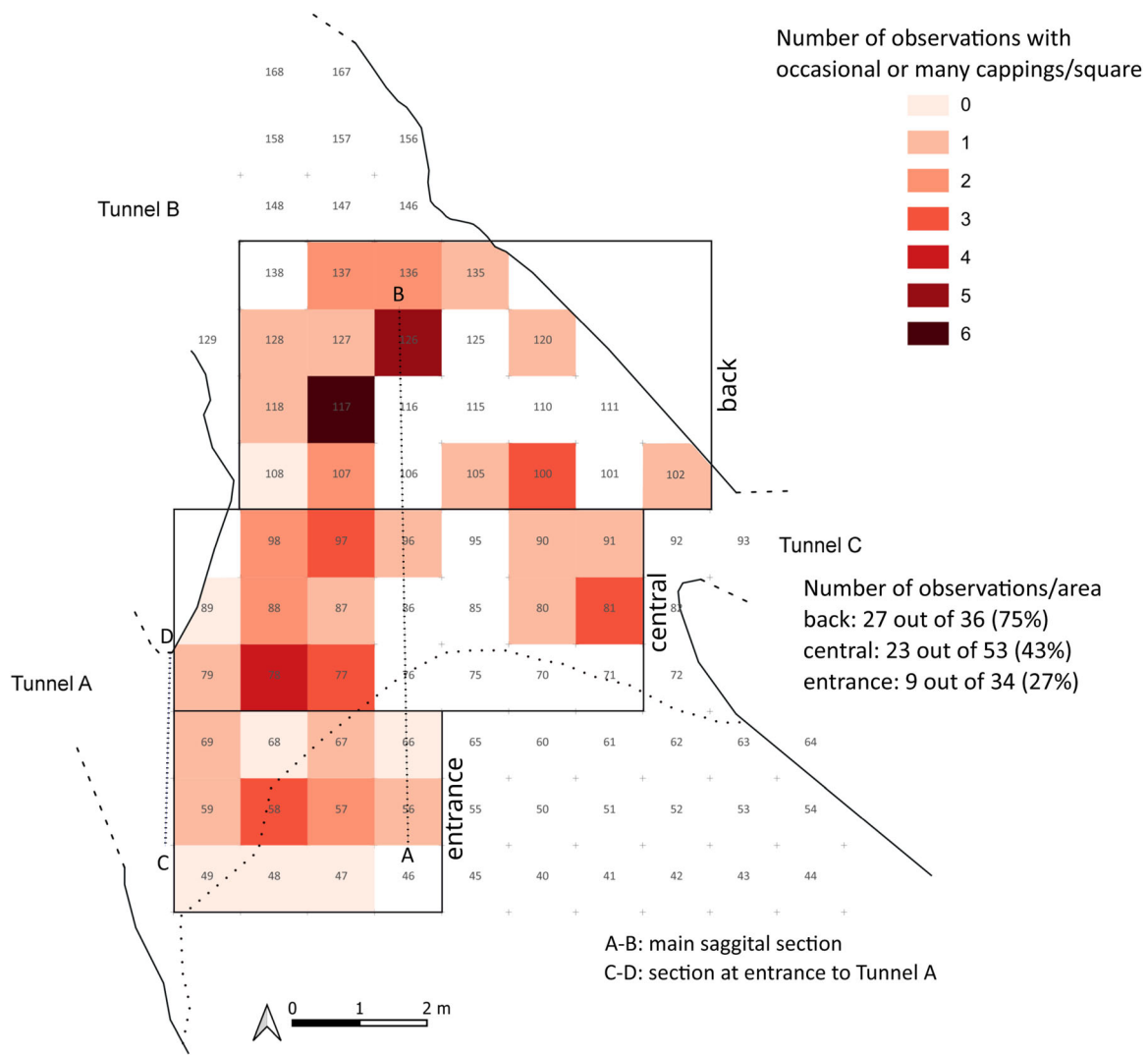


FIGURE 13 | Origin of thin sections with occasional or many silt cappings ($n = 59$).

Admixtures of silt size quartz and mica grains as well as silicate clay particles probably derived from eolian inputs (Cremaschi et al. 2005). Higher proportions of these particles are indicated by clay loam and loam textures of units A2, A3, and A10, and deposition of aeolian dust is generally increased in external zones of the cave. Diachronic change in the dust sedimentation rate is difficult to deduce because of spatial heterogeneity in dust deposition and difficulties of chronological dating (s. below).

Theoretically, deposition of silt and clay could also be explained by sheet flow entering the cave through the entrance or via cracks in the cave roof. The sediments do not show any macro- or microscopic signatures of laminated bedding or cross bedding; hence, higher velocity surface runoff enabling transport and separation of sand- from silt-sized grains or even fine gravel probably did not enter the cave. The interbedding of sandy and loamy sediments observed in thin section A4 MM8 could reflect intermittent accumulation of sands from the cave roof and of finer facies by subaqueous deposition as observed during excavation. However, this thin section derives from an anthropogenic sediment feature, and it is not unlikely that such interbedding originates from anthropogenic dumping of different

substrates or accidental import of loamy deposits from outside the cave. Overall, field evidence and micromorphological features suggest that water-lain deposition of sediments did not play a significant role in the aggradation of the sequence.

Anthropogenic deposition of charcoal, bone, and lithics was particularly high in the case of A1, A2, A5–A6, and A9–A11 and included many sedimentary features (Marcazzan et al. 2023). From a micromorphological perspective, the proportion of anthropogenic materials outside features of Fumane is mostly low. Few thin sections show higher amounts of these materials and/or have a dark gray groundmass due to enrichment with burned residues. Further anthropogenic imprints consist of abundant red mineral pigment in thin sections from subunit A2R and in ash layers of some anthropogenic sediment features from units A2, A6, and A10. Several previously assumed combustion features are now classified as occupation horizons and isolated concentrations of anthropogenic materials (Marcazzan et al. 2023). Overall, relatively high amounts of anthropogenic materials were found in front of tunnel A, which is the most intensively studied part of the cave. Additional hotspots of human activity could not be identified with the selection of thin sections studied. The lack or low amounts of archaeological

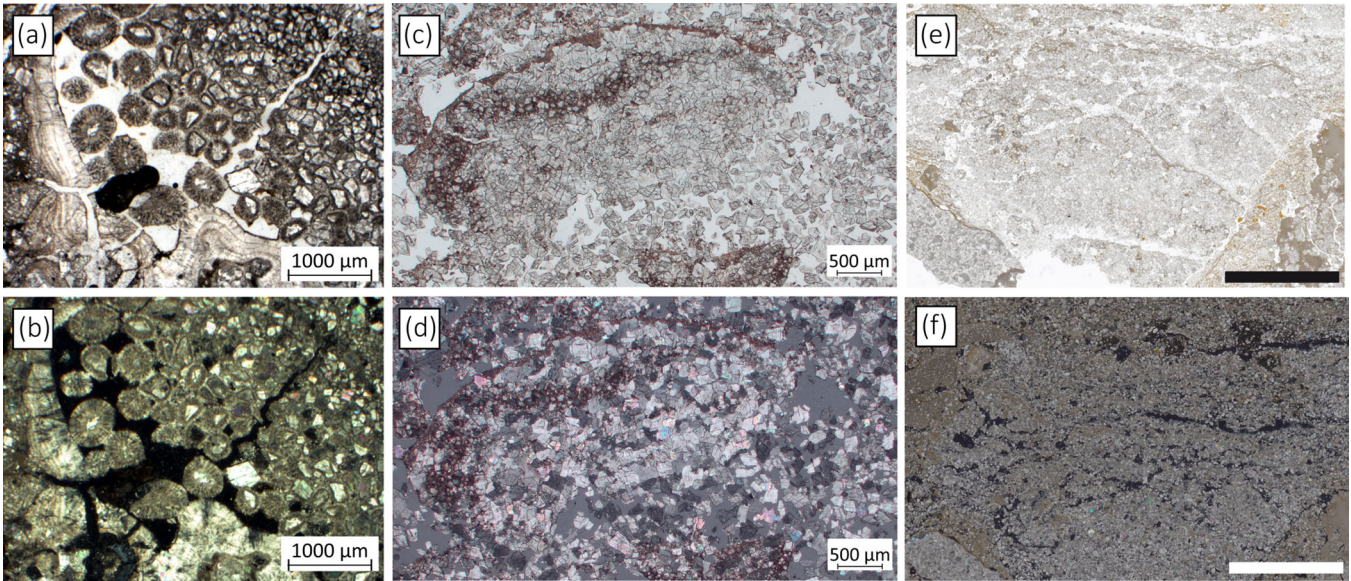


FIGURE 14 | (a, b) Rare occurrence of dissolution hollows within limestone fragment under PPL and XPL, respectively (thin section A4 MM4). (c, d) Mechanically disintegrating dolostone fragment in thin section A7 MM2 under PPL and partially crossed polarizers, respectively. (e, f) Flatbed scan of disintegrating rock fragment in A7 MM2 under transmitted ordinary light and using two polarization foils, respectively. Scale bars in flatbed scans equal 10 mm in length.

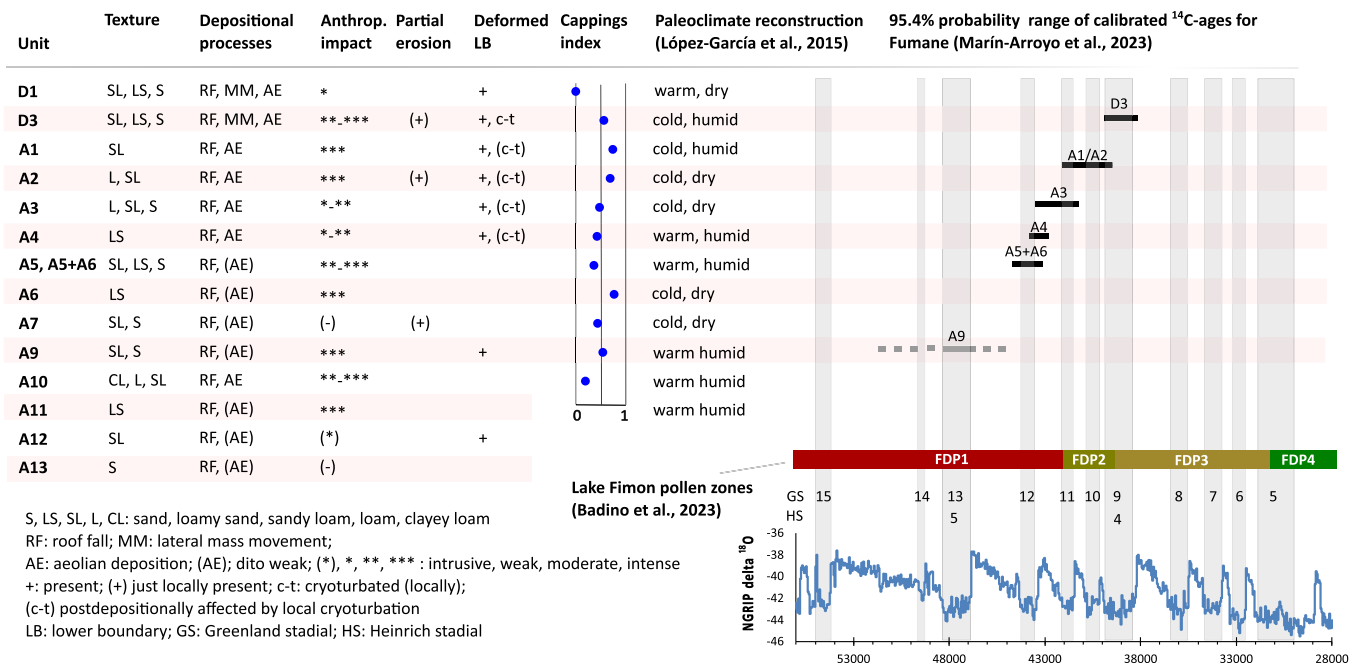


FIGURE 15 | Major depositional and postdepositional natural processes and anthropogenic contribution (acc. to Table 1) in the upper Fumane sedimentary sequence. The silt cappings index reflects the abundance of cappings. Paleoclimate reconstruction of López-García based on microfaunal evidence from Fumane. Modeled calibrated ¹⁴C data ranges at a 95% confidence interval of each archaeological unit as based on the radiocarbon data compilation of Marín-Arroyo et al. (2023) and using OxCAL 4.4 (Bronk Ramsey 2009) and the IntCal20 calibration curve (Reimer et al. 2020). The age range of A9 is poorly constrained (Badino et al. 2023). NorthGrip delta ¹⁸O curve, timing of Greenland interstadials and stadials (Rasmussen et al. 2014), and Heinrich stadials (Sanchez Goñi and Harrison 2010) for comparison.

materials in units D1, D3, A3, A4, and A7, however, clearly suggest that occupation did not reach the intensities of other times or was even interrupted (A7, A12–13). Among those layers, the archaeologically sterile unit A7 represents an excellent model for accumulation of sediment with no or very limited human impact (Supporting Information S1: Figures S1.8–S1.10).

5.2 | Syn- and Postdepositional Alteration

During and after the accumulation of single layers, sediments of Fumane were subject to limited structural and compositional changes. Ripple-like upper surfaces of layers or partial layer truncation within units A7 and A2 as well as topographic

depressions filled with sediments during later accumulation phases suggest episodic events of erosion by internal cave flow. Hydraulic activity was also responsible for partial erosion of D3 β . Topographic depressions may have formed by animal use of the cave, which, during accumulation of A7, was probably responsible for the partial truncation of A9 and formation of a fold-like (Supporting Information S1: Figure S1.9D) depression propagating toward the inner cave. In addition, a marmot tunnel was exposed during excavation, cutting through sediments of unit A10 to A5+A6 (e.g., Supporting Information S1: Figures S1.3 and S1.12D). However, loss of sediments by hydraulic erosion or animal use of the cave is very limited.

Undulating sedimentary boundaries, intermixing of materials from different layers, and inverse stratification are indicators of further postdepositional deformation processes. Field evidence for units A5+A6 to A2, including the strongly turbated subunit A2R, suggests that parts of these units were affected by cryoturbation, that is, the deformation of sediments by freeze–thaw–related expansion and contracting and mixing of sediments, implying a phase of pronounced soil frost within the cave or at least in its inner eastern zone after the accumulation of these layers. However, microscopic effects of cryoturbation such as ductile or brittle deformation structures in pedofeatures or circular orientation of components (Van der Meer and Menzies 2011; Pawelec et al. 2015; Mùcher et al. 2018; Van Vliet-Lanoë and Cox 2018) were not recorded in thin sections from Fumane. This lack may partly relate to insufficient samples from cryoturbated layers and/or weak micromorphological imprint of cryoturbation in the sandy deposits of Fumane.

During accumulation of unit D3, sliding boulders and slabs (Supporting Information S1: Figure S1.1) exerted differential compaction and traction on underlying subunits D3a+b and A2 (Supporting Information S1: Figures S1.1A and S1.2C). Here, mass movements caused deformation of the underlying sediments, accompanied by small-scale upward and downward displacement of lithics across the layers defined during fieldwork (Falcucci et al. 2024). Finally, sediment deformation at Fumane may have been caused by unevenly distributed load exerted by falling rock slabs, bioturbation, or cryoturbation, and finally also by anthropogenic mixing and deformation of the living floor. Some of these processes may be responsible for deformation features such as undulating lower boundaries of A2 and A6 in the center-east of the cave (Supporting Information S1: Figure S1.3) as well as in A9 and A11 (Table 1, Figure 15), vertically arranged stones with densely spaced deformations, and intrusions of anthropogenic material from A11 in A12 and A13 or intrusions of artifacts into A7 from A6. Deformation of sediments thus occurred within the cave during several phases, but intense cryoturbation was restricted to the back part of the cave and probably took place during accumulation of D3 β , the uppermost unit showing clear cryoturbation features.

Other postdepositional processes were effective on a microscale. The locally high degree of compaction may relate to trampling (Rentzel et al. 2017; Miller 2017; Karkanis and Goldberg 2019), which is also indicated by crushed bone identified in some of the features and postulated as a major process for the formation of occupation horizons and laminated anthropogenic features in Fumane (Marcazzan et al. 2023). However, compaction can

also result from ice lensing (Van Vliet-Lanoë and Cox 2018), but this process is probably of minor importance in Fumane, as discussed below. It should be noted that the gravelly sands to loamy sands present in most thin sections of Fumane do not represent substrates susceptible to compaction (Karkanis and Goldberg 2019) and effects of trampling or frost may not be recorded well.

A large proportion of pores inspected under the microscope are biogenic and probably related to small soil mesofauna and fine plant roots. Beside the marmot burrow, field evidence and micromorphological features suggest that burrowing activity mostly took place on a microscale. Except for disturbances in human-made sediment features (Marcazzan et al. 2023) and the erosion or cryoturbation-affected parts, the sedimentary sequence is thus characterized by stratigraphic integrity. This is also indicated by the fact that silt cappings are almost always located on the top of limestone fragments, which argues against considerable reworking of the clasts.

Most layers show weak chemical weathering of limestone clasts. Physical disintegration of the surrounding dolostone was probably the dominant process of limestone weathering and limited physical degradation after deposition of clasts on the cave floor occurred as well.

The dissolution of carbonate within the substrate and precipitation of secondary carbonates are two processes that are not necessarily proportional to each other. Besides leaching within the deposit, the source of secondary calcite may be droppings of bicarbonate-rich waters from the cave walls and roof. Relatively high amounts of secondary carbonates in the entrance zone near the present drip line may indicate that the dripping source is important, but the location of the drip line before collapse of the roof before and during the Last Glacial is not known. The diffuse carbonate enrichment would fit into a spatio-temporally variable dripping pattern from the roof. On the other hand, rare hypocoatings formed by uptake of soil water by fine plant roots, leaving micrite enriched groundmass around the pore behind, suggest the former presence of fine plant roots and precipitation of carbonate from bicarbonate-rich pore water in their vicinity.

Most sediments have abundant and large pores allowing quick percolation of water from snowmelt, rainfall, dripping from the cave roof, or after rare events of surface runoff or karstic seepage possibly entering the cave. Percolating water can transport fine mineral grains downward. During transport, the particles may be filtered out on larger mineral grains or in ending pores, where thin clay and silt bridges between sand grains, cappings on coarser grains, or thick coatings of pores can form (Kühn et al. 2018) depending on the intensity of the translocation processes. The presence of silt cappings testifies to the redistribution of silt and clay within sediments of Fumane cave. Transport distance was likely short, as indicated by the color of the cappings, which is identical to the color of the neighboring groundmass. A significant downward transport from one layer to the other, as known for clay illuviation processes in soils (Kühn et al. 2018), probably did not take place. This is indicated by the low abundance of silt cappings in units A7 and A10, which are overlain by layers comparatively rich in silt cappings. That most of the cappings are found on the

upward-facing surfaces of coarse grains attests to the dominance of vertical transport and argues against later mechanical disturbance of the sedimentary context. Short transport in the carbonate-rich sediments may relate to high electrolyte concentrations in pore water inhibiting the dispersion of silicate clays. In fact, the poor layering within silt cappings suggests that clay particles were transported in coagulated mode. The formation of silt cappings in each thin section is probably also related to local differences in the porosity of the deposits and the presence of large filtering surfaces such as dolostone fragments and other coarse materials, including bone and lithics embedded in the porous groundmass. In Fumane, silt cappings appear to be more strongly developed in layers underlying the loosely packed pore-rich 'sabbie' (sand) facies, which may be related to higher amounts of percolating water. Overall, the heterogeneity of sediment properties governing filtering surfaces and water percolation causes a high spatial variability of silt capping formation within each stratigraphic unit.

5.3 | Paleoclimatic Implications

Evidence for overall cold climatic conditions during the accumulation of Fumane sequence is high abundances of angular and subangular platy limestone clasts (Table 1). This frost-shattered debris accumulated in all units of Fumane, apparently without any strong changes in intensity if we exclude unit A12 (mostly sandy) and the westernmost and outermost areas of the cave, due to the lithology of the wall or the lack of the roof, respectively.

When excavating units A1–A3, and A6–A7 vertically tilted stones, mechanical deformations of the layer interfaces, dispersion, and microbreakage of artifacts and other were observed in the East area of the cave entrance (Supporting Information S1: Figures S1.15 and S1.16a–c). It appears likely that these features were caused by gelifluction and cryoturbation requiring cold temperatures and sufficient moisture enabling annual freeze–thaw cycles in the sediments. The local expression of these features possibly relates to different microclimatic zones in the former cavity, with more pronounced frost near the W- and NW-facing wall of the cave.

Silt cappings, banded fabric, and granular and platy microstructures are common micromorphological features observed in frost-affected paleosols, Fragipans, or well-drained coarse-grained Arctic soils. These features have been related to repeated freeze–thaw cycles under periglacial climate conditions (Kühn et al. 2018; Van Vliet-Lanoë and Cox 2018) and are also found in last glacial sediments of caves and rockshelters such as in Lusarkert cave, Armenia, and Ortvala Klde, Georgia (Mallol and Goldberg 2017; Brittingham et al. 2019), Geißenklösterle and Hohle Fels in Swabia (Goldberg et al. 2003; Miller 2015; Goldberg et al. 2019), or Jarama VI and Abrigo del Molino in Central Iberia (Kehl et al. 2013, 2018). Considering the weak expression of frost-related features such as banded fabrics or platy microstructures and limited macroscopic frost signals in Fumane, it appears likely that temperature changes inside Fumane cave were rather modest and strong frost-related effects, including the formation of ice lenses mainly restricted to accumulation of unit D3, when cryoturbation affected part of the deposit.

However, silt cappings at Fumane are well expressed in some layers, being most abundant in units D3, A1/A2, and A5–A6 (Figure 15). Although differential expression of silt cappings could be related to changes in frost within the cave, differences in precipitation-related percolation rates or variation of snowfall relative to rainfall should also be considered. As mentioned above, the high porosity of sediments in Fumane allows fast percolation of water, favoring the local redistribution of fine particles. Besides mobilization of silt by direct rainfall at the surface of the cave floor, snowfall meltwater with low electrolyte concentrations may have promoted dispersion of clay particles, breakdown of microaggregates, and lateral or vertical movement of silt and clay. Though probably not promoting the formation of ice lensing in the whole cave environment of Fumane, the postulated temperature depressions for the area (see below) make it likely that snowfall was increased during stadial (and probably interstadial) periods of MIS 3. Silt cappings were observed even in the back part of Fumane Cave. Snow may have been blown inside these areas behind the drip line, and then snowfall meltwater could have been responsible for the translocation of silt and clay. In the Fumane Cave context, silt capping formation can thus be explained by moisture and temperature changes. Less cappings were formed during phases of reduced percolation of pore water during dry and/or warm (less snowfall) phases, concomitant with accumulation of units A10, A9, A7, and A4–A3. Silt cappings will have formed if relatively moist and/or cold conditions (more snowfall) enabled higher percolation of pore water and filtration of silt, which could have been the case during accumulation of units A5–A6, A2, and A1 as well as D3 showing increased silt capping abundance.

Furthermore, spatially variable factors, such as the preferential dripping of water on the cave floor or lateral variation in porosity and granulometry, affect the percolation intensity and the filtering potential of fine grains, adding to the high spatial variability of silt capping expression in Fumane. Considering the weak expression of other frost-related features such as banded fabrics or platy microstructures and limited macroscopic frost signals in Fumane, it appears likely that temperature changes inside Fumane cave were rather modest and strong frost-related effects, including the formation of ice lenses mainly restricted to accumulation of unit D3, when cryoturbation affected part of the deposit. The discussion of paleoclimate imprints in the Fumane sequence should also consider that cave systems and rockshelters are protected environments with lower amplitudes in temperature and humidity than in their surroundings (e.g., Liu et al. 2017); hence, climate signals recorded in the cave may reflect higher amplitude climate change outside.

5.4 | Comparison With Climate Proxy Records of Northern Italy

Several studies identified frost-related features in last glacial sediment sequences bordering the Po plain in Northern Italy, although with discontinuous evidence (see Peresani et al. 2021). Platy and locally banded microstructure, widespread occurrence of silt cappings on rock fragments, and disrupted and reworked clay coatings were described for unit 15 of Ciota Ciara

cave (Angelucci et al. 2019), located at 665 m asl in the western Piedmont of the Southern Alps. Cremaschi and van Vliet-Lanoë (1990) report on frost-shattered debris, cryogenic breccia, and micromorphological evidence of frost activity, including platy to subangular blocky structure, in the Middle Paleolithic layers of Tagliente shelter, situated at 250 m asl about 10 km to the southeast of Fumane. The same study reports on the presence of frost features in several loess profiles located in the wider area. For the sites mentioned, the timing of frost feature formation is not well constrained, and correlation with MIS 3 is unclear. Further to the south at Arene Candide, a platy microstructure was recorded in Gravettian layers correlated with HS 3 (Rellini et al. 2013), hence after accumulation of the relevant sequence at Fumane.

The available radiocarbon dates for Fumane suggest that accumulation of units A5 and A5+A6 mainly occurred during Greenland Stadial (GS) 12 and continued into Greenland Interstadial (GI) 11, during which A4 and A3 formed, the latter extending until GI 10 and showing a temporal overlap with A1/A2 (Figure 15). D3 probably falls into GS 9, equivalent to HS 4, which was possibly the coldest period during MIS 3 in the Po plain (Badino et al. 2023). The accumulation period from the Late Mousterian unit A5+A6 to Protoaurignacian unit D3 is thus placed from c. 45–38 ka, providing a chronological framework for correlation with climate archives of the wider area. Paleoenvironmental reconstructions using small-mammal remains at Fumane suggest relatively cold conditions in the habitats of insectivores, bats, and rodents during accumulation of units A7 to A6 and A3 to A1 (López-García et al. 2015; Figure 15). These climate signals were correlated with Heinrich Events (HE) 5 and 4, that is, phases of massive iceberg releases into the Northern Atlantic (Heinrich 1988; Bond et al. 1992; López-García et al. 2015). Increased formation of silt cappings was observed in units A6 and A2, A2R, and A1, which may partly correlate with these postulated cold periods. However, according to López-García et al. (2015), the mean annual temperature at Fumane cave was maximally reduced by 5.9°C compared to the current values at the meteorological station Verona-Villafranca (12.4°C), located at 68 m asl, thus ~200 m below Fumane Cave. The mean temperatures of the coldest month decreased by a maximum of 2.9°C, down to -1.4°C. The reconstructed temperature depression for the coldest months during cold periods is thus not high. In addition, the difference in temperature reduction between postulated relatively cold and warm phases is rather weak, fitting with the moderate changes in silt capping expression. López-García et al. (2015) also estimated that the MAP during accumulation of units A11–D1e was as high as 1305–1448 mm, hence c. 438–621 mm higher than the present-day value (827 mm at Verona-Villafranca), and that the cold periods defined above were characterized by less rainfall than the warm periods. Differences between ‘dry’ and ‘humid’ phases are, however, less than 150 mm in MAP, thus being negligible for the postulated permanently humid climate during MIS 3 (López-García et al. 2015).

Detailed paleoenvironmental reconstructions for the Po plain were produced on a pollen record base from Lake Fimon, located in the Berici hills 40 km east from Fumane (Pini et al. 2010; Badino et al. 2020, Badino et al. 2023). In accordance with paleoclimate modeling (Barron and Pollard 2002), lower

MAP during MIS 3 than at present was revealed. The Lake Fimon pollen sequence reflects a mosaic of boreal forest and steppe with temperate trees, including *Tilia* and *Abies* (Pini et al. 2010), indicating a significantly dryer and colder climate than today. Opening of the forest documented in pollen zone FPD 17c suggests a major change toward still colder and drier conditions possibly correlating with HS4 (Pini et al. 2010). A recent high-resolution pollen study from the same lacustrine basin (Badino et al. 2023) further refines the reconstruction of vegetation types in the upper Po plain. Plant taxa in pollen zone FDP1 (60–42 ka) reflect a mosaic of dry boreal forest, cool-temperate mixed forest, steppe, and desert steppe as well as other grasslands, including meadow steppe, suggesting open cool-temperate woodlands. Pollen zone FDP2 (42–39 ka) is characterized by increased shares of grassland documenting a further opening of the landscape and step toward even drier climate conditions. Although the vegetation change related to FDP2 sets in with GS 11, it appears likely that it culminates with HS 4. Interestingly, limited modern vegetation analogs were identified for the pollen spectra of FDP2, stressing its unique composition of grassland, cool-temperature mixed forest, and dry boreal forests. In pollen zone FDP3 (39–31 ka), boreal forest and steppe taxa again expanded, whereas taxa of other grassland and cool-temperate mixed forests were less. FDP4 (31–28 ka) reflects an increase in boreal dry forest at the expense of other vegetation types. The cold and dry phases reflected by FDP2 thus appear to reflect the coldest and driest period.

During MIS 3, the continental lowlands of Northern Italy thus experienced relatively modest temperature and moisture changes (Badino et al. 2020), with a major peak in dryness and cold during HS4. The mostly moderate temperature-related effects on the sedimentary sequence of Fumane, except for deformation of units D3, and A1–A7 by local cryoturbation fit this picture.

6 | Conclusions

Detailed field descriptions and micromorphological study of macro-units A and D at Fumane provide new insights into the composition and structure of sediments, providing information on depositional processes, postdepositional alterations, and stratigraphic integrity of the site during the Middle to Upper Paleolithic transition. The sediments originate from physical disintegration of the dolostone cave roof and walls and to a lesser degree from eolian inputs and anthropogenic materials. Anthropogenic sedimentation outside of sediment features is low to moderate; effects of trampling are rarely identified.

Further depositional and postdepositional processes include the accumulation of secondary calcite and physical redistribution of silt and micromass to form silt cappings. The spatial distribution of silt cappings within the cave and information from climate records of the area may suggest that their formation is related to increased snowmelt. Considering the weak expression of other frost-related features, ice lensing in the cave sediments is unlikely to have played a significant role. The formation of silt cappings was most pronounced during accumulation of units A1, A2 and A5–A6, and possibly enhanced by decreases in

temperature culminating during HS 4, when solifluction and cryoturbation affected the sequence.

The thickness, gravel content, and granulometry of the fine fraction of each unit may spatially vary to a large degree, as is known from field observations. It is thus not surprising that thin sections from the same unit also show a large variation in micromorphological properties. Sampling ideally covers this variation, but due to technical reasons, this is often not possible. Overall, field and micromorphological observations compare fairly well and confirm the stratigraphic integrity of most parts of the sequence.

Behind the background of more or less continuous supply of frost-shattered rubble, diachronic change in the expression of pedofeatures probably relates to moisture changes rather than strong temperature effects. The micromorphological observations thus support the notion that human occupation at Fumane took place under rather temperate climate conditions without a strong variation in seasonal frost.

Author Contributions

Martin Kehl: conceptualization (lead), investigation (lead), writing – original draft, review and editing (lead), funding acquisition. **Diana Marazzan:** investigation (supporting), visualization (supporting), writing – review and editing (equal). **Armando Faluccci:** writing – review and editing (equal), visualization (equal). **Christopher E. Miller:** writing – review and editing (equal). **Rossella Duches:** investigation (supporting), resources (equal). **Marco Peresani:** conceptualization (lead), investigation (supporting), writing – original draft, review and editing (equal), funding acquisition.

Acknowledgments

The authors acknowledge the constructive comments of two anonymous reviewers that helped to significantly improve the manuscript. They thank Panagiotis Kritikakis (Senckenberg Centre for Human Evolution and Palaeoenvironment [HEP], Tübingen, Germany) for producing new thin sections from unit A10. Moreover, they are grateful to the entire working team of Fumane Cave, especially to Mauro Cremaschi, who co-directed together with Alberto Broglio the excavations at Fumane from 1989 to 1997 and identified the main stratigraphic units. The excavation is coordinated by the University of Ferrara (M. Peresani), with the collaboration of Italian and European research institutions and with the support of the Ministry of Cultural Heritage— Archaeological Superintendence SAPAB, public institutions (Regional Natural Park, B.I.M. Adige, Municipality of Fumane), private associations, and companies. M.K. was supported by the German Research Foundation (project 408333614; KE 818/8-1). Open Access funding enabled and organized by Projekt DEAL.

Conflicts of Interest

The authors declare no conflicts of interest.

References

Aguzzi, M., A. Amorosi, M. L. Colalongo, et al. 2007. “Late Quaternary Climatic Evolution of the Arno Coastal Plain (Western Tuscany, Italy) From Subsurface Data.” *Sedimentary Geology* 202, no. 1–2, SI: 211–229. <https://doi.org/10.1016/j.sedgeo.2007.03.004>.

Alcaraz-Castaño, M., J. Alcolea-González, M. Kehl, et al. 2017. “A Context for the Last Neandertals of Interior Iberia: Los Casares Cave Revisited.” *PLoS One* 12, no. 7: e0180823. <https://doi.org/10.1371/journal.pone.0180823>.

Angelucci, D. E., M. Zambaldi, U. Tessari, et al. 2019. “New Insights on the Monte Fenera Palaeolithic, Italy: Geoarchaeology of the Ciota Ciara Cave.” *Geoarchaeology* 34, no. 4: 413–429. <https://doi.org/10.1002/gea.21708>.

Badino, F., R. Pini, C. Ravazzi, et al. 2020. “An Overview of Alpine and Mediterranean Palaeogeography, Terrestrial Ecosystems and Climate History During MIS 3 With Focus on the Middle to Upper Palaeolithic Transition.” *Quaternary International* 551: 7–28. <https://doi.org/10.1016/j.quaint.2019.09.024>.

Badino, F., R. Pini, C. Ravazzi, et al. 2023. “High-Resolution Ecosystem Changes Pacing the Millennial Climate Variability at the Middle to Upper Palaeolithic Transition in NE-Italy.” *Scientific Reports* 13, no. 1: 12478. <https://doi.org/10.1038/s41598-023-38081-1>.

Barron, E., and D. Pollard. 2002. “High-Resolution Climate Simulations of Oxygen Isotope Stage 3 in Europe.” *Quaternary Research* 58, no. 3: 296–309. <https://doi.org/10.1006/qres.2002.2374>.

Bartolomei, G., A. Broglio, P. Cassoli, et al. 1992. “La Grotte-Abri de Fumane.” *Un site Aurignacien au Sud des Alps. Preistoria Alpina* 28: 131–179.

Blasi, C., G. Chirici, P. Corona, M. Marchetti, F. Maselli, and N. Puletti. 2007. “Spatialization of Climatic Data at the Italian National Level by Local Regressive Models.” *Forest@ - Rivista Di Selvicoltura Ed Ecologia Forestale* 4, no. 2: 213–219. <https://doi.org/10.3832/efor0453-0040213>.

Bond, G., H. Heinrich, W. Broecker, et al. 1992. “Evidence for Massive Discharges of Icebergs Into the North Atlantic Ocean During the Last Glacial Period.” *Nature* 360, no. 6401: 245–249. <https://doi.org/10.1038/360245a0>.

Brittingham, A., M. T. Hren, G. Hartman, et al. 2019. “Geochemical Evidence for the Control of Fire by Middle Palaeolithic Hominins.” *Scientific Reports* 9, no. 1: 15368. <https://doi.org/10.1038/s41598-019-51433-0>.

Bronk Ramsey, C. 2009. “Bayesian Analysis of Radiocarbon Dates.” *Radiocarbon* 51, no. 1: 337–360. <https://doi.org/10.1017/S0033822200033865>.

Brönnimann, D., C. Pümpin, K. Ismail-Meyer, P. Rentzel, and N. Égüez. 2017. “Excrement of Omnivores and Carnivores.” In *Archaeological Soil and Sediment Micromorphology*. Edited by N. Cristiano and S. Georges, 67–81. John Wiley & Sons, Ltd. <https://doi.org/10.1002/9781118941065.ch7>.

Canti, M. G. 2003. “Aspects of the Chemical and Microscopic Characteristics of Plant Ashes Found in Archaeological Soils.” *CATENA* 54, no. 3: 339–361. [https://doi.org/10.1016/S0341-8162\(03\)00127-9](https://doi.org/10.1016/S0341-8162(03)00127-9).

Cavallo, G., F. Fontana, S. Gialanella, et al. 2018. “Heat Treatment of Mineral Pigment During the Upper Palaeolithic in North-East Italy.” *Archaeometry* 60, no. 5: 1045–1061. <https://doi.org/10.1111/arc.12360>.

Cavallo, G., F. Fontana, F. Gonzato, M. Peresani, M. P. Riccardi, and R. Zorzin. 2017. “Textural, Microstructural, and Compositional Characteristics of Fe-Based Geomaterials and Upper Paleolithic Ocher in the Lessini Mountains, Northeast Italy: Implications for Provenance Studies.” *Geoarchaeology* 32, no. 4: 437–455. <https://doi.org/10.1002/gea.21617>.

Colagè, I., and F. d’Errico. 2020. “Culture: The Driving Force of Human Cognition.” *Topics in Cognitive Science* 12, no. 2: 654–672. <https://doi.org/10.1111/tops.12372>.

Courty, M. A. 2001. “Microfacies Analysis Assisting Archaeological Stratigraphy.” In *Earth Sciences and Archaeology*. Edited by P. Goldberg, V. T. Holliday, and C. R. Ferring, 205–239. Springer US. https://doi.org/10.1007/978-1-4615-1183-0_8.

Courty, M. A., P. Goldberg, and R. I. MacPhail. 1989. *Soils and Micromorphology in Archaeology*. Cambridge University Press.

Courty, M. A., and J. Vallverdu. 2001. “The Microstratigraphic Record of Abrupt Climate Changes in Cave Sediments of the Western Mediterranean.” *Geoarchaeology* 16, no. 5: 467–499. <https://doi.org/10.1002/gea.1002>.

- Cremaschi, M., F. Ferraro, M. Peresani, and A. Tagliacozzo. 2005. "Il sito: nuovi contributi sulla stratigrafia, la cronologia, le faune a macromammiferi e le industrie del paleolitico antico." In *Memorie Museo Civico Storia Naturale di Verona: Vol. 9. Pitture paleolitiche nelle Prealpi Venete: Grotta di Fumane e Riparo Dalmeri*. Edited by A. Broglio and G. Dalmeri, 12–22. Italy: Museo delle Scienze.
- Cremaschi, M., and B. van Vliet-Lanoë. 1990. "Traces of Frost Activity and Ice Segregation in Pleistocene Loess Deposits and Till of Northern Italy: Deep Seasonal Freezing or Permafrost?" *Quaternary International* 5: 39–48. [https://doi.org/10.1016/1040-6182\(90\)90023-W](https://doi.org/10.1016/1040-6182(90)90023-W).
- Dansgaard, W., S. J. Johnsen, H. B. Clausen, et al. 1993. "Evidence for General Instability of Past Climate From a 250-kyr Ice-Core Record." *Nature* 364, no. 6434: 218–220. <https://doi.org/10.1038/364218a0>.
- D'Errico, F., and W. E. Banks. 2013. "Identifying Mechanisms Behind Middle Paleolithic and Middle Stone Age Cultural Trajectories." supplement, *Current Anthropology* 54, no. S8: S371–S387. <https://doi.org/10.1086/673388>.
- Douka, K., T. F. G. Higham, R. Wood, et al. 2014. "On the Chronology of the Uluzzian." *Journal of Human Evolution* 68: 1–13. <https://doi.org/10.1016/j.jhevol.2013.12.007>.
- Durand, N., H. C. Monger, M. G. Canti, and E. P. Verrechia. 2018. "Chapter 9—Calcium Carbonate Features." In *Interpretation of Micromorphological Features of Soils and Regoliths*. Edited by G. Stoops, V. Marcelino, and F. Mees, 205–258. Elsevier. <https://doi.org/10.1016/B978-0-444-63522-8.00009-7>.
- Estévez, J., X. S. Villagran, A. L. Balbo, and K. Hardy. 2014. "Microtaphonomy in Archaeological Sites: The Use of Soil Micromorphology to Better Understand Bone Taphonomy in Archaeological Contexts." *Quaternary International* 330: 3–9. <https://doi.org/10.1016/j.quaint.2013.08.007>.
- Falcucci, A., N. J. Conard, and M. Peresani. 2017. "A Critical Assessment of the Protoaurignacian Lithic Technology at Fumane Cave and Its Implications for the Definition of the Earliest Aurignacian." *PLoS One* 12, no. 12: e0189241. <https://doi.org/10.1371/journal.pone.0189241>.
- Falcucci, A., D. Giusti, F. Zangrossi, M. De Lorenzi, L. Ceregatti, and M. Peresani. 2024. "Refitting the Context: A Reconsideration of Cultural Change Among Early *Homo sapiens* at Fumane Cave Through Blade Break Connections, Spatial Taphonomy, and Lithic Technology." *Journal of Paleolithic Archaeology* 8: 2. <https://doi.org/10.1007/s41982-024-00203-0>.
- Falcucci, A., and M. Peresani. 2019. "A Pre-Heinrich Event 3 Assemblage at Fumane Cave and Its Contribution for Understanding the Beginning of the Gravettian in Italy." *Quartär* 66: 135–154. https://doi.org/10.7485/QU66_6.
- Ferraro, F. 2009. "Age, Sedimentation, and Soil Formation in the Val Sorda Loess Sequence, Northern Italy." *Quaternary International* 204, no. 1–2: 54–64. <https://doi.org/10.1016/j.quaint.2008.12.002>.
- Goldberg, P., and F. Berna. 2010. "Micromorphology and Context." *Quaternary International* 214, no. 1–2: 56–62. <https://doi.org/10.1016/j.quaint.2009.10.023>.
- Goldberg, P., and R. I. Macphail. 2006. *Practical and Theoretical Geoarchaeology*. John Wiley & Sons Ltd. <https://doi.org/10.1002/9781118688182>.
- Goldberg, P., C. E. Miller, and N. J. Conard. 2019. "Geißenklösterle Stratigraphy and Micromorphology." In *Tübinger Monographien zur Urgeschichte. Geißenklösterle: Chronostratigraphie, Paläoumwelt und Subsistenz im Mittel- und Jungpaläolithikum der Schwäbischen Alb = Geißenklösterle: Chronostratigraphie, Paläoumwelt und Subsistenz During the Middle and Upper Paleolithic of the Swabian Jura*. Edited by N. J. Conard, M. Bolus, and S. C. Münzel. Kerns Verlag, 25–62.
- Goldberg, P., C. E. Miller, S. Schiegl, et al. 2009. "Bedding, Hearths, and Site Maintenance in the Middle Stone Age of Sibudu Cave, KwaZulu-Natal, South Africa." *Archaeological and Anthropological Sciences* 1, no. 2: 95–122. <https://doi.org/10.1007/s12520-009-0008-1>.
- Goldberg, P., S. Schiegl, K. Meline, C. Dayton, and N. J. Conard. 2003. "Micromorphology and Site Formation at Hohle Fels Cave, Schwabian Jura, Germany." *E&G Quaternary Science Journal* 53, no. 1: 1–25. <https://doi.org/10.3285/eg.53.1.01>.
- Greenbaum, G., D. E. Friesem, E. Hovers, M. W. Feldman, and O. Kolodny. 2019. "Was Inter-Population Connectivity of Neanderthals and Modern Humans the Driver of the Upper Paleolithic Transition Rather Than Its Product?" *Quaternary Science Reviews* 217: 316–329. <https://doi.org/10.1016/j.quascirev.2018.12.011>.
- Heinrich, H. 1988. "Origin and Consequences of Cyclic Ice Rafting in the Northeast Atlantic Ocean During the Past 130,000 Years." *Quaternary Research* 29, no. 2: 142–152. [https://doi.org/10.1016/0033-5894\(88\)90057-9](https://doi.org/10.1016/0033-5894(88)90057-9).
- Higham, T., F. Brock, M. Peresani, A. Broglio, R. Wood, and K. Douka. 2009. "Problems With Radiocarbon Dating the Middle to Upper Palaeolithic Transition in Italy." *Quaternary Science Reviews* 28, no. 13–14: 1257–1267. <https://doi.org/10.1016/j.quascirev.2008.12.018>.
- Higham, T., K. Douka, R. Wood, et al. 2014. "The Timing and Spatio-temporal Patterning of Neanderthal Disappearance." *Nature* 512, no. 7514: 306–309. <https://doi.org/10.1038/nature13621>.
- Higham, T., R. Jacobi, L. Basell, C. B. Ramsey, L. Chiotti, and R. Nespoulet. 2011. "Precision Dating of the Palaeolithic: A New Radiocarbon Chronology for the Abri Pataud (France), a Key Aurignacian Sequence." *Journal of Human Evolution* 61, no. 5: 549–563. <https://doi.org/10.1016/j.jhevol.2011.06.005>.
- Horwitz, L. K., and P. Goldberg. 1989. "A Study of Pleistocene and Holocene Hyaena Coprolites." *Journal of Archaeological Science* 16, no. 1: 71–94. [https://doi.org/10.1016/0305-4403\(89\)90057-5](https://doi.org/10.1016/0305-4403(89)90057-5).
- Hublin, J. J. 2015. "The Modern Human Colonization of Western Eurasia: When and Where?" *Quaternary Science Reviews* 118: 194–210. <https://doi.org/10.1016/j.quascirev.2014.08.011>.
- Karkanas, P., K. S. Brown, E. C. Fisher, Z. Jacobs, and C. W. Marean. 2015. "Interpreting Human Behavior From Depositional Rates and Combustion Features Through the Study of Sedimentary Microfacies at Site Pinnacle Point 5-6, South Africa." *Journal of Human Evolution* 85: 1–21. <https://doi.org/10.1016/j.jhevol.2015.04.006>.
- Karkanas, P., and P. Goldberg. 2013. "6.23 Micromorphology of Cave Sediments." In *Treatise on Geomorphology*. Edited by J. F. Shroder, 286–297. Academic Press. <https://doi.org/10.1016/B978-0-12-374739-6.00120-2>.
- Karkanas, P., and P. Goldberg. 2019. *Reconstructing Archaeological Sites: Understanding the Geoarchaeological Matrix*. Wiley Blackwell. <http://search.ebscohost.com/login.aspx?direct=true&scope=site&db=nlebk&AN=1831025>.
- Kehl, M., D. Álvarez-Alonso, M. De Andrés-Herrero, et al. 2018. "The Rock Shelter Abrigo del Molino (Segovia, Spain) and the Timing of the Late Middle Paleolithic in Central Iberia." *Quaternary Research* 90: 180–200. <https://doi.org/10.1017/qua.2018.13>.
- Kehl, M., C. Burow, P. Cantalejo, et al. 2016. "Site Formation and Chronology of the New Paleolithic Site Sima de Las Palomas de Teba, Southern Spain." *Quaternary Research* 85: 313–331. <https://doi.org/10.1016/j.yqres.2016.01.007>.
- Kehl, M., C. Burow, A. Hilgers, et al. 2013. "Late Neanderthals at Jarama VI (Central Iberia)?" *Quaternary Research* 80, no. 2: 218–234. <https://doi.org/10.1016/j.yqres.2013.06.010>.
- Kooistra, M. J., and M. M. Pulleman. 2018. "Chapter 16—Features Related to Faunal Activity." In *Interpretation of Micromorphological Features of Soils and Regoliths*. Edited by G. Stoops, V. Marcelino, and F. Mees, 447–469. Elsevier. <https://doi.org/10.1016/B978-0-444-63522-8.00016-4>.
- Kühn, P., J. Aguilar, R. Miedema, and M. Bronnikova. 2018. "Chapter 14—Textural Pedofeatures and Related Horizons." In *Interpretation of*

- Micromorphological Features of Soils and Regoliths. Edited by G. Stoops, V. Marcelino, and F. Mees, 377–423. Elsevier. <https://doi.org/10.1016/B978-0-444-63522-8.00014-0>.
- Linstädter, J., and M. Kehl. 2012. “The Holocene Archaeological Sequence and Sedimentological Processes at IFRI Oudadane, NE Morocco.” *Journal of Archaeological Science* 39: 3306–3323. <https://doi.org/10.1016/j.jas.2012.05.025>.
- Liu, W., C. Zhou, Z. Liu, C. Yang, and A. Brancelj. 2017. “The Temperature Variation in an Epikarstic Cave and Its Impact Factors: A Case From Velika Pasica Cave, Central Slovenia.” *Arabian Journal of Geosciences* 10, no. 1: 2. <https://doi.org/10.1007/s12517-016-2761-7>.
- López-García, J. M., C. dalla Valle, M. Cremaschi, and M. Peresani. 2015. “Reconstruction of the Neanderthal and Modern Human Landscape and Climate From the Fumane Cave Sequence (Verona, Italy) Using Small-Mammal Assemblages.” *Quaternary Science Reviews* 128: 1–13. <https://doi.org/10.1016/j.quascirev.2015.09.013>.
- Mallol, C., D. Cabanes, and J. Baena. 2010. “Microstratigraphy and Diagenesis at the Upper Pleistocene Site of Esquilieu Cave (Cantabria, Spain).” *Quaternary International* 214, no. 1–2: 70–81. <https://doi.org/10.1016/j.quaint.2009.10.018>.
- Mallol, C., and P. Goldberg. 2017. “Cave and Rock Shelter Sediments.” In *Archaeological Soil and Sediment Micromorphology*. Edited by C. Nicosia and G. Stoops, 359–381. John Wiley & Sons, Ltd. <https://doi.org/10.1002/9781118941065.ch34>.
- Mallol, C., and S. M. Mentzer. 2017. “Contacts Under the Lens: Perspectives on the Role of Microstratigraphy in Archaeological Research.” *Archaeological and Anthropological Sciences* 9, no. 8: 1645–1669. <https://doi.org/10.1007/s12520-015-0288-6>.
- Marcazzan, D., C. E. Miller, B. Ligouis, R. Duches, N. J. Conard, and M. Peresani. 2023. “Middle and Upper Paleolithic Occupations of Fumane Cave (Italy): A Geoarchaeological Investigation of the Anthropogenic Features.” *Journal of Anthropological Sciences = Rivista di antropologia: JASS* 101: 37–62. <https://doi.org/10.4436/JASS.10002>.
- Marín-Arroyo, A. B., G. Terlato, M. Vidal-Cordasco, and M. Peresani. 2023. “Subsistence of Early Anatomically Modern Humans in Europe as Evidenced in the Protoaurignacian Occupations of Fumane Cave, Italy.” *Scientific Reports* 13, no. 1: 3788. <https://doi.org/10.1038/s41598-023-30059-3>.
- van der Meer, J. J. M., and J. Menzies. 2011. “The Micromorphology of Unconsolidated Sediments.” *Sedimentary Geology* 238, no. 3–4: 213–232. <https://doi.org/10.1016/j.sedgeo.2011.04.013>.
- Miller, C. E. 2015. *A Tale of Two Swabian Caves: Geoarchaeological Investigations at Hohle Fels and Geißenklösterle*. Tübingen Publications in Prehistory. Kerns.
- Miller, C. E. 2017. “Trampling.” In *Encyclopedia of Geoarchaeology*. Edited by A. S. Gilbert, 981–982. Springer Netherlands. https://doi.org/10.1007/978-1-4020-4409-0_128.
- Miller, C. E., P. Goldberg, and F. Berna. 2013. “Geoarchaeological Investigations at Diepkloof Rock Shelter, Western Cape, South Africa.” *Journal of Archaeological Science* 40, no. 9: 3432–3452. <https://doi.org/10.1016/j.jas.2013.02.014>.
- Mücher, H., H. van Steijn, and F. Kwaad. 2018. “Chapter 2—Colluvial and Mass Wasting Deposits.” In *Interpretation of Micromorphological Features of Soils and Regoliths*. Edited by G. Stoops, V. Marcelino, and F. Mees, 21–36. Elsevier. <https://doi.org/10.1016/B978-0-444-63522-8.00002-4>.
- Munsell Color. 2009. Munsell Soil Color Charts.
- Nicosia, C. and Stoops, G., eds. 2017. *Archaeological Soil and Sediment Micromorphology*. Wiley. <http://onlinelibrary.wiley.com/book/10.1002/9781118941065>.
- North American Commission on Stratigraphic Nomenclature. 2005. “North American Stratigraphic Code.” *AAPG Bulletin* 89, no. 11: 1547–1591.
- Pawelec, H., M. Drewnik, and M. Żyła. 2015. “Paleoenvironmental Interpretation Based on Macro- and Microstructure Analysis of Pleistocene Slope Covers: A Case Study From the Miechów Upland, Poland.” *Geomorphology* 232: 145–163. <https://doi.org/10.1016/j.geomorph.2014.12.012>.
- Peresani, M. 2012. “Fifty Thousand Years of Flint Knapping and Tool Shaping Across the Mousterian and Uluzzian Sequence of Fumane Cave.” *Quaternary International* 247: 125–150. <https://doi.org/10.1016/j.quaint.2011.02.006>.
- Peresani, M. 2022. “Inspecting Human Evolution From a Cave. Late Neanderthals and Early Sapiens at Grotta Di Fumane: Present State and Outlook.” *Journal of Anthropological Sciences = Rivista Di Antropologia: JASS* 100: 71–107. <https://doi.org/10.4436/JASS.10016>.
- Peresani, M., S. Bertola, D. Delpiano, S. Benazzi, and M. Romandini. 2019. “The Uluzzian in the North of Italy: Insights Around the New Evidence at Riparo Broion.” *Archaeological and Anthropological Sciences* 11, no. 7: 3503–3536. <https://doi.org/10.1007/s12520-018-0770-z>.
- Peresani, M., J. Chrzavzez, A. Danti, et al. 2011. “Fire-Places, Frequentations and the Environmental Setting of the Final Mousterian at Grotta di Fumane: A Report From the 2006–2008 Research.” *Quartär* 58: 131–151. https://doi.org/10.7485/QU58_07.
- Peresani, M., M. Cremaschi, F. Ferraro, et al. 2008. “Age of the Final Middle Palaeolithic and Uluzzian Levels at Fumane Cave, Northern Italy, Using ¹⁴C, ESR, ²³⁴U/²³⁰Th and Thermoluminescence Methods.” *Journal of Archaeological Science* 35, no. 11: 2986–2996. <https://doi.org/10.1016/j.jas.2008.06.013>.
- Peresani, M., E. Cristiani, and M. Romandini. 2016. “The Uluzzian Technology of Grotta di Fumane and Its Implication for Reconstructing Cultural Dynamics in the Middle–Upper Palaeolithic Transition of Western Eurasia.” *Journal of Human Evolution* 91: 36–56. <https://doi.org/10.1016/j.jhevol.2015.10.012>.
- Peresani, M., D. Delpiano, R. Duches, et al. 2017. “Il Musteriano delle unità A10 e A11 a Grotta di Fumane (VR). Risultati delle campagne di scavo 2014 e 2016.” *FastiOnline Documents & Research* 397: 1–13.
- Peresani, M., G. Monegato, C. Ravazzi, et al. 2021. “Hunter-Gatherers Across the Great Adriatic-Po Region During the Last Glacial Maximum: Environmental and Cultural Dynamics.” *Quaternary International* 581–582: 128–163. <https://doi.org/10.1016/j.quaint.2020.10.007>.
- Pini, R., C. Ravazzi, and M. Donegana. 2009. “Pollen Stratigraphy, Vegetation and Climate History of the Last 215 ka in the Azzano Decimo Core (Plain of Friuli, North-Eastern Italy).” *Quaternary Science Reviews* 28, no. 13–14: 1268–1290. <https://doi.org/10.1016/j.quascirev.2008.12.017>.
- Pini, R., C. Ravazzi, and P. J. Reimer. 2010. “The Vegetation and Climate History of the Last Glacial Cycle in a New Pollen Record From Lake Fimon (Southern Alpine Foreland, N-Italy).” *Quaternary Science Reviews* 29, no. 23–24: 3115–3137. <https://doi.org/10.1016/j.quascirev.2010.06.040>.
- Rasmussen, S. O., M. Bigler, S. P. Blockley, et al. 2014. “A Stratigraphic Framework for Abrupt Climatic Changes During the Last Glacial Period Based on Three Synchronized Greenland Ice-Core Records: Refining and Extending the INTIMATE Event Stratigraphy.” *Quaternary Science Reviews* 106: 14–28. <https://doi.org/10.1016/j.quascirev.2014.09.007>.
- Reimer, P. J., W. E. N. Austin, E. Bard, et al. 2020. “The IntCal20 Northern Hemisphere Radiocarbon Age Calibration Curve (0–55 cal kBP).” *Radiocarbon* 62, no. 4: 725–757. <https://doi.org/10.1017/RDC.2020.41>.
- Rellini, I., M. Firpo, G. Martino, J. Riel-Salvatore, and R. Maggi. 2013. “Climate and Environmental Changes Recognized by Micromorphology in Paleolithic Deposits at Arene Candide (Liguria, Italy).” *Quaternary International* 315: 42–55. <https://doi.org/10.1016/j.quaint.2013.05.050>.
- Rentzel, P., C. Nicosia, A. Gebhardt, et al. 2017. “Trampling, Poaching and the Effect of Traffic.” In *Archaeological Soil and Sediment*

Micromorphology. Edited by C. Nicosia, G. Stoops, 281–297. John Wiley & Sons Ltd. <https://doi.org/10.1002/9781118941065.ch30>.

Rivas-Martínez, S., S. Rivas Sáenz, and A. Penas Merino. 2011. “Worldwide Bioclimatic Classification System.” *Glob Geobot* 1: 1–634. <https://doi.org/10.5616/gg110001>.

Sanchez Goñi, M. F., and S. P. Harrison. 2010. “Millennial-Scale Climate Variability and Vegetation Changes During the Last Glacial: Concepts and Terminology.” *Quaternary Science Reviews* 29, no. 21–22: 2823–2827. <https://doi.org/10.1016/j.quascirev.2009.11.014>.

Slimak, L., C. Zanolli, T. Higham, et al. 2022. “Modern Human Incur-sion Into Neanderthal Territories 54,000 Years Ago at Mandrin, France.” *Science Advances* 8, no. 6: eabj9496. <https://doi.org/10.1126/sciadv.abj9496>.

Spötl, C., A. Mangini, and D. A. Richards. 2006. “Chronology and Palaeoenvironment of Marine Isotope Stage 3 From Two High-Elevation Speleothems, Austrian Alps.” *Quaternary Science Reviews* 25, no. 9–10: 1127–1136. <https://doi.org/10.1016/j.quascirev.2005.10.006>.

Stoops, G. 2021. “Guidelines for Analysis and Description of Soil and Regolith Thin Sections.” In *ASA, CSSA, and SSSA Bks.* 2nd ed., American Society of Agronomy. Edited by M. J. Vepraskas, 240. Wiley. <https://doi.org/10.1002/9780891189763>.

Stoops, G., Marcelino, V., and Mees, F., eds. 2018. *Interpretation of Micromorphological Features of Soils and Regoliths*. Elsevier.

Vaesen, K., G. L. Dusseldorp, and M. J. Brandt. 2021. “An Emerging Consensus in Palaeoanthropology: Demography Was the Main Factor Responsible for the Disappearance of Neanderthals.” *Scientific Reports* 11, no. 1: 4925. <https://doi.org/10.1038/s41598-021-84410-7>.

Villa, P., and W. Roebroeks. 2014. “Neandertal Demise: An Archaeological Analysis of the Modern Human Superiority Complex.” *PLoS One* 9, no. 4: e96424. <https://doi.org/10.1371/journal.pone.0096424>.

Van Vliet-Lanoë, B., and C. A. Cox. 2018. “Chapter 20—Frost Action.” In *Interpretation of Micromorphological Features of Soils and Regoliths*, (2nd ed.) Edited by G. Stoops, V. Marcelino, and F. Mees, 575–603. Elsevier. <https://doi.org/10.1016/B978-0-444-63522-8.00020-6>.

Voelker, A. H. L. 2002. “Global Distribution of Centennial-Scale Records for Marine Isotope Stage (MIS) 3: A Database.” *Quaternary Science Reviews* 21, no. 10: 1185–1212. [https://doi.org/10.1016/S0277-3791\(01\)00139-1](https://doi.org/10.1016/S0277-3791(01)00139-1).

Wacha, L., and M. Frechen. 2011. “The Geochronology of the “Gorjanović Loess Section” in Vukovar, Croatia.” *Quaternary International* 240, no. 1–2: 87–99. <https://doi.org/10.1016/j.quaint.2011.04.010>.

Zilhão, J., F. d’Errico, W. E. Banks, and N. Teyssandier. 2024. “A Data-Driven Paradigm Shift for the Middle-to-Upper Palaeolithic Transition and the Neandertal Debate.” *Quaternary Environments and Humans* 2: 100037. <https://doi.org/10.1016/j.qeh.2024.100037>.

Supporting Information

Additional supporting information can be found online in the Supporting Information section.